frontiers | Frontiers in Batteries and Electrochemistry

TYPE Review
PUBLISHED 08 March 2024
DOI 10.3389/fbael.2024.1369305

OPEN ACCESS

EDITED BY
Xingcheng Xiao,
General Motors, United States

REVIEWED BY
Yifan Zhao,
General Motors, United States
John Vaughey,
Argonne National Laboratory (DOE),
United States

*CORRESPONDENCE
Ryan C. Hill,
ryan.c.hill@stonybrook.edu

RECEIVED 12 January 2024
ACCEPTED 29 February 2024
PUBLISHED 08 March 2024

CITATION
Hill RC, Gross MS, Percival SJ, Peretti AS, Small LJ, Spoerke ED and Cheng Y-T (2024), Molten sodium batteries: advances in chemistries, electrolytes, and interfaces. *Front. Batteries Electrochem.* 3:1369305. doi: 10.3389/fbael.2024.1369305

Molten sodium batteries: advances in chemistries, electrolytes, and interfaces

Ryan C. Hill[1,2]*, Martha S. Gross[3], Stephen J. Percival[3], Amanda S. Peretti[3], Leo J. Small[3], Erik D. Spoerke[3] and Yang-Tse Cheng[1]

[1]Department of Chemical and Materials Engineering, University of Kentucky, Lexington, KY, United States, [2]The Institute of Energy: Sustainability, Environment, and Equity, Stony Brook University, Stony Brook, NY, United States, [3]Sandia National Laboratories, Albuquerque, NM, United States

The need for clean, renewable energy has driven the expansion of renewable energy generators, such as wind and solar. However, to achieve a robust and responsive electrical grid based on such inherently intermittent renewable energy sources, grid-scale energy storage is essential. The unmet need for this critical component has motivated extensive grid-scale battery research, especially exploring chemistries "beyond Li-ion". Among others, molten sodium (Na) batteries, which date back to the 1960s with Na-S, have seen a strong revival, owing mostly to raw material abundance and the excellent electrochemical properties of Na metal. Recently, many groups have demonstrated important advances in battery chemistries, electrolytes, and interfaces to lower material and operating costs, enhance cyclability, and understand key mechanisms that drive failure in molten Na batteries. For widespread implementation of molten Na batteries, though, further optimization, cost reduction, and mechanistic insight is necessary. In this light, this work provides a brief history of mature molten Na technologies, a comprehensive review of recent progress, and explores possibilities for future advancements.

KEYWORDS

sodium batteries, grid storage, solid electrolytes, interfaces, ZEBRA, Na-S

1 Introduction

Energy use is a foundational aspect of human society. However, the continued use of non-renewable fossil fuels, such as oil, coal, and natural gas, is unsustainable (Burnham and Braun, 1990; Cross and Phillips, 1990; Perera, 2017; Kreps, 2020; Arnold and Osborne, 2023). Furthermore, their combustion releases carbon dioxide gas that accumulates in the atmosphere and leads to global warming (Archer et al., 2009; Andres et al., 2012; Ediger, 2019). The harmful effects of fossil fuels have led to the development of new, renewable methods to generate electricity. Namely, wind and solar energy have emerged as promising options to address the global energy crisis (Ackermann and Söder, 2000; Mekhilef et al., 2011). Wind turbines are spun solely with the power of wind, eliminating the need for steam turbines that rely on fossil fuels (Balat, 2009). Photovoltaic panels are composed of semiconducting materials that absorb energetic photons from the Sun and excite electrons that can then flow and generate electricity (El Chaar et al., 2011). Neither of these methods require fossil fuels to harness energy and their expansion significantly reduces the carbon footprint left by electricity generation (Bhandari et al., 2020; Lu et al.,

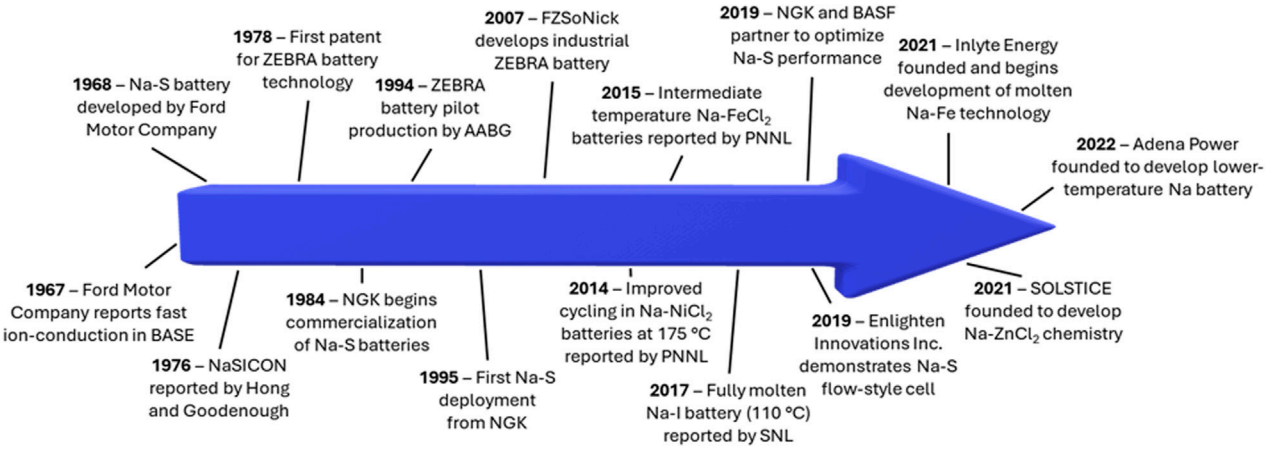

FIGURE 1
Timeline of important research and commercial efforts to advance molten Na batteries.

2023). Importantly, these clean energy sources not only serve to replace fossil fuels for electricity generation, but they offer routes to satisfy growing demands for vehicle and industrial electrification (Yuan et al., 2021). These transformative new demands for clean, around-the-clock electricity stand to strain the existing grid infrastructure.

Additionally, both wind and solar suffer from intermittent and variable electricity generation (Anvari et al., 2016). Although the total energy harvested by wind and solar would be sufficient to support many critical industry sectors, significant amounts of energy may be wasted due to fluctuating, mismatched supply and demand, or limitations on the ability to transmit and distribute the energy when and where it is needed (Islam et al., 2014). Fossil fuels are then still necessary to supply an agile and reliable energy supply during times of peak demand or unplanned outages (Jebaselvi and Paramasivam, 2013; Calero et al., 2022). To combat fluctuating supply and demand and to relieve transmission congestion issues, many renewable generators utilize energy storage to reclaim energy that would be lost during periods of peak production, and to maintain a stable, responsive energy supply during periods of peak demand (Anvari et al., 2016; Kosowatz, 2018; Moran et al., 2018; Denholm et al., 2020; Rahman et al., 2020; Calero et al., 2022). In addition to short-term energy management (2–4 h), there is hope that long-duration energy storage (LDES) (>10–12 h) can strengthen the electrical grid during extended generation outages to further reduce reliance on fossil fuels (Albertus et al., 2020; Guerra, 2021; International Energy Agency, 2022; Long Duration Energy Storage Council, 2022; Denholm et al., 2023). Moreover, electrification of the transportation and industrial manufacturing sectors, which add significant load to the electrical grid, will absolutely require large-scale, extended-duration storage to meet energy demands (Pereirinha et al., 2018; Wei et al., 2019).

Rechargeable batteries are a promising energy storage solution. (Zhu et al., 2022a). Since the commercialization of the lithium-ion battery in the 1990s, battery-powered devices have become an integral part of society (Nagaura, 1990). However, lithium-ion batteries can encounter issues with materials supply chains, safety, and most importantly, cost (Helbig et al., 2018a; Helbig et al., 2018b; Wentker et al., 2019a; Wentker et al., 2019b; Karabelli et al., 2020; Chen et al., 2021; Kebede et al., 2021). This has led to exploration of many "beyond Li-ion" battery chemistries, which rely on cheaper, more sustainable materials. Molten sodium (Na) batteries, which were first introduced with the Na-sulfur (S) battery in the 1960s, are promising for grid-scale energy storage due to the widespread abundance of Na resources and the desirable electrochemical properties of Na metal (1,166 mA h g^{-1}, -2.71 V vs. SHE) (Kummer and Weber, 1968; Coetzer, 1986; Karabelli et al., 2020). Their potential for effective grid-scale storage has led to the recent revitalization of molten Na battery research, with many groups tackling issues related to cost, lifetime, and energy/power density. This research progress has ignited commercialization efforts for various molten Na chemistries, by companies such as Enlighten Innovations, Inlyte Energy, Solstice, and Adena Power. This review aims to highlight recent progress and important remaining challenges in the field of molten Na batteries. Some important research and commercialization efforts are highlighted in Figure 1. Clear from this figure is the fact that although molten Na batteries have been in development for decades, the increased focus on these technologies in the last 10 years reveals a revitalization of this promising, Na-based set of technologies.

2 Early molten Na batteries

2.1 Na-S batteries

Na-S batteries were first developed in the 1960s by the Ford Motor Company (Kummer and Weber, 1968). Na-S cells couple an elemental S positive electrode with the Na negative electrode. The S electrode may be composited with carbon or absorbed in a carbon sponge to improve electronic conduction within the electrode. Traditionally, these cells were operated in excess of 300 °C, where the S electrode is also molten (Kummer and Weber, 1968; Weiner, 1977; Sudworth and Tilley, 1986). The two molten electrodes mandate a solid electrolyte to provide electrode containment, ion conduction, and electron blockage (Yung-Fang Yu and Kummer,

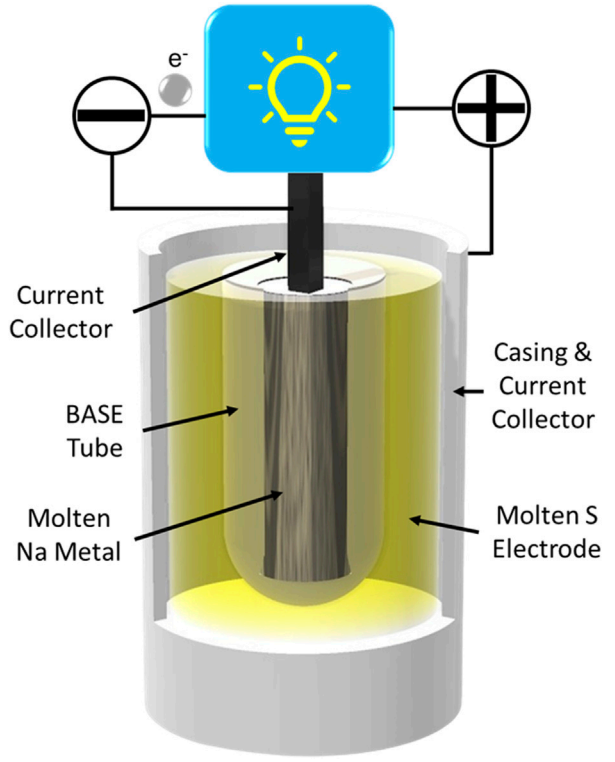

FIGURE 2
Illustration of a tubular molten Na-S battery configuration using a β″-alumina solid electrolyte (BASE).

1967; Whittingham and Huggins, 1971a; Whittingham and Huggins, 1971b). Traditionally, β″-alumina, $Na_{1+x}Al_{11}O_{17+x/2}$, $_xAl_{11}O_{17+x/2}$, where x is typically ~0.3, served as the electrolyte for early Na-S batteries (Yung-Fang Yu and Kummer, 1967; Kummer and Weber, 1968). The non-stoichiometric nature of the β″-alumina solid electrolyte (hereafter referred to as BASE) is due to the presence of mobile Na^+ that allow ion passage between electrodes. A typical configuration of a tubular molten Na-S cell is illustrated in Figure 2.

During discharge of Na-S batteries, Na metal at the negative electrode is oxidized to Na^+ ions. These ions pass through the BASE and react with the sulfur electrode to form a series of sodium polysulfides, ranging from Na_2S_8 to Na_2S_2. However, Na_2S_2 solidifies and cannot be reverted to elemental sulfur upon charging, so discharge should be ceased before any Na_2S_2 is formed. The negative and positive half-cell reactions and overall cell reaction are listed in Eqs 1–3.

$$Na\,(l) \leftrightarrow Na^+ + e^- \tag{1}$$

$$xS\,(l) + 2e^- \leftrightarrow S_x^{2-} \tag{2}$$

$$2Na\,(l) + xS\,(l) \leftrightarrow Na_2S_x\,(s\,or\,l) \tag{3}$$

Since these reactions occur in sequential stages, the potential at each composition slightly changes. An average voltage of ~2.0 V is produced from these reactions (Kummer and Weber, 1968; Weiner, 1977; Sudworth and Tilley, 1986).

Na-S batteries have been successfully commercialized for grid-scale storage by NGK Insulators, LTD, and they have deployed 720 MW/4.9 GWh of storage around the world in more than 200 cities (Spoerke et al., 2030). NGK provides batteries that possess energy and power densities of 367 Wh L^{-1} and 36 W kg^{-1}, respectively, and can achieve cycle lives of ~4,500 cycles (NGL-Insulator, 2023). However, their high temperature operation (above 300°C) and engineering measures to address the hazardous reactivity of sodium and sulfur led to elevated operating costs and historically limited their application (Ohi, 1992; National Research Council, 2012; NGL-Insulator, 2023). Through a recent partnership between NGK and chemical manufacturer BASF, these batteries have been further optimized to improve lifetimes (7,300 projected cycles) and reduce costs (NAS Batteries, 2023).

2.2 ZEBRA batteries

In the 1980s, the first Na metal halide (NaMH) batteries were developed under the Zero-Emission Battery Research Activities (ZEBRA) project (Coetzer, 1986). This chemistry sought to improve upon the Na-S battery. ZEBRA batteries also use molten sodium metal negative electrodes and BASE as the solid electrolyte. However, the positive electrode of a ZEBRA battery consists of a molten sodium tetrachloroaluminate ($NaAlCl_4$) salt mixed with $NiCl_2$ (and, sometimes, $FeCl_2$) particles. The $NaAlCl_4$, which is often referred to as a secondary electrolyte or catholyte, melts near 154 °C and helps to alleviate the issue of ionic conductivity of Na^+ in the positive electrode (Coetzer, 1986; Bones et al., 1989; Sudworth, 2001). The early ZEBRA battery configuration is similar to a Na-S cell, with the S electrode (e.g., as shown in Figure 2) replaced by the halide salt/catholyte mixture. The half-cell reactions for the positive electrode are listed in Eqs 4, 5. Note that the negative half-cell reaction is the same as the Na-S chemistry (Eq. 1).

$$NiCl_2\,(s) + 2Na^+ + 2e^- \rightarrow Ni\,(s) + 2NaCl\,(s) \tag{4}$$

$$FeCl_2\,(s) + 2Na^+ + 2e^- \rightarrow Fe\,(s) + 2NaCl\,(s) \tag{5}$$

The primary $NiCl_2$ reaction leads to a voltage plateau near 2.58 V, while the $FeCl_2$ (if included) reaction occurs at a plateau near 2.35 V (Coetzer, 1986; Bones et al., 1989; Sudworth, 2001). These typically occur sequentially, with the $NiCl_2$ discharging first, followed by the $FeCl_2$ discharge. These two separate plateaus can be useful for gauging the SOC of the battery. $FeCl_2$ addition can also serve to reduce the internal resistance of the cell, increasing the power (high current) capability of ZEBRA batteries. At high current, the polarization within ZEBRA batteries may be high enough that the voltage plateau is below 2.35 V and both reactions occur simultaneously (Dustmann, 2004; Sakaebe et al., 2014).

Besides the higher voltage, ZEBRA batteries are believed to be inherently safer than Na-S, requiring fewer engineering controls to address the hazardous reactivity of high temperature molten Na and S. If the ceramic electrolyte in a ZEBRA battery were to fail (a phenomenon that will be discussed in detail later) the reaction between Na metal and $NaAlCl_4$ (Eq. 6):

$$Na\,(l) + NaAlCl_4\,(l) \rightarrow 4NaCl\,(s) + Al\,(s) \tag{6}$$

produces only benign salt and Al metal, and is far less violent than the reaction between Na and S (Trickett, 1998; Dustmann, 2004;

TABLE 1 Comparison of commercialized molten Na energy technologies with other chemistries. Information for other chemistries sourced from the World Energy Council.

Chemistry	Temperature	Max lifetime	Energy density	Power rating	Efficiency (%)
Na-S (NGK) NGL-Insulator (2023)	300°C–340°C	4,500 cycles	367 Wh L^{-1}	36 W kg^{-1}	
Na-MH (FZSoNick) Fzsonick (2023b)	250°C	4,500 cycles	90 Wh L^{-1}		90
Li-ion Gardner et al. (2016)	RT	10,000 cycles	200–400 Wh L^{-1}	100 MW	85–95
Lead-acid Gardner et al. (2016)	RT	1,000 cycles	50–80 Wh L^{-1}	100 MW	80–90
V redox flow Gardner et al. (2016)	RT	14,000 cycles	20–70 Wh L^{-1}	100 MW	60–85

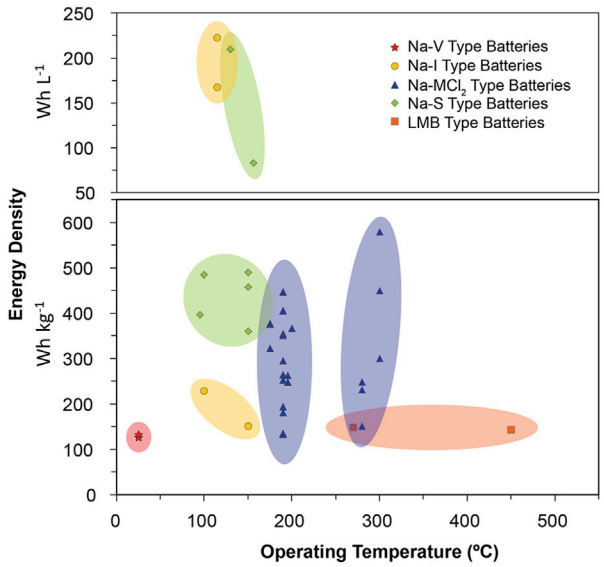

FIGURE 3
Gravimetric and volumetric energy densities of recent molten Na battery reports. Numeric values for points in the figure are included in Table 2.

Sakaebe et al., 2014) Moreover, the high Na^+ conductivity afforded by the $NaAlCl_4$ catholyte allows for a slight reduction in temperature, with ZEBRA batteries capable of operating near 250°C. $NaAlCl_4$ also prevents chlorine gas formation if the battery is overcharged through a secondary reaction (Eq. 7) with Ni metal:

$$2NaAlCl_4(l) + Ni(s) \rightarrow NiCl_2(s) + Na(l) + 2AlCl_3(l) \quad (7)$$

Finally, ZEBRA batteries can be assembled in the discharged state, where it is not necessary to handle air and moisture-sensitive Na metal.

Traditional ZEBRA batteries have been successfully commercialized by FZSoNick and have found a niche in grid-scale as well as select mobile storage applications, totaling 500 MWh of total storage (Fzsonick, 2023a; Spoerke et al., 2030). These batteries provide an energy density of ~90 Wh L^{-1}, attain cycle lives up to 4,500 cycles at 80% depth of discharge (DOD), and display total energy efficiencies near 90% (accounting for the energy needed to maintain their operating temperature) (Fzsonick, 2023b). One common concern with ZEBRA batteries is the inclusion of Ni metal, which has a relatively high "supply risk" (SR - a score from 0 to 100 that quantifies a material's susceptibility to supply concerns). This is mainly attributed to its high and increasing demand, which is partially fueled by its extensive use in Li-ion batteries (Helbig et al., 2018a; Wentker et al., 2019a). As with Na-S, it is desirable to lower costs by reducing the operating temperature of ZEBRA batteries, but this is limited by two factors. Firstly, the catholyte becomes viscous at lower temperatures and solidifies below 154°C, eliminating the high Na^+ conductivity in the positive electrolyte and compromising the ability to cycle reliably (Bones et al., 1989). Secondly, the conductivity of the BASE exponentially decreases with decreasing temperature (Kummer, 1972; Dustmann, 2004). Potential remedies to these issues for ZEBRA batteries and their descendants are addressed in the following sections. Table 1 compares commercial Na-S and ZEBRA battery systems to other current energy storage technologies (as described by the World Energy Council) (Gardner et al., 2016).

3 Next-generation molten sodium batteries

Significant research has recently been conducted to improve molten Na batteries, particularly for grid-scale energy storage. Figure 3 illustrates recently reported gravimetric and volumetric energy densities of various chemistries as a function of temperature (numeric values for these points are included in Table 2) (Parthasarathy et al., 2007; Lu et al., 2013a; Lu et al., 2013b; Li et al., 2013; Lu et al., 2014; Kim et al., 2015a; Li et al., 2015a; Shamie et al., 2015; Spatocco et al., 2015; Li et al., 2016a; Liu et al., 2016; Xu et al., 2016; Ao et al., 2017a; Chang et al., 2017; Holzapfel et al., 2017; Small et al., 2017; Xue et al., 2017; Chang et al., 2018a; Chang et al., 2018b; Jung et al., 2018; Lu et al., 2018; Yang et al., 2018; Ahn et al., 2019; Jin et al., 2019a; Nikiforidis et al., 2019; Niu et al., 2019; Ding et al., 2020a; Gross et al., 2020a; Li et al., 2020a; Zhan et al., 2020a; Ding et al., 2020b; Zhan et al., 2020b; Gao et al., 2020; Gross et al., 2021; Niu et al., 2021; Wang et al., 2021; Flynn et al., 2022; Zhou et al., 2022; Heinz et al., 2023; Lan et al., 2023; Weller et al., 2023) To reduce operating and material costs, lower temperature molten Na batteries are the most desirable. As such, ZEBRA-style batteries have garnered more recent attention than their Na-S counterparts, due to the higher melting points of sodium/sulfur compounds, as well as the safer inherent reactivity of the ZEBRA molten salts. However, Figure 3 shows that Na-S type batteries, and various other chemistries, are also promising for next-generation molten Na batteries. Newer chemistries, such as a higher voltage Na-I battery, liquid metal batteries (LMBs), and Na flow batteries (NFBs) have been developed and promise to lower costs while maintaining the necessary energy densities for grid-scale storage.

TABLE 2 Summary of performance metrics in recent molten Na battery publications. Energy densities marked with * were estimated based on information available in the publications. In Electrolyte column, S, L, and MS indicates solid, liquid, or molten salt, respectively. For any blank entries, information was not provided or able to be calculated.

Year reference	Chemistry	Temp. (°C)	Electrolyte	Energy density	Cycle life
2013 Lu et al. (2013a)	Na-S/$NiCl_2$	280	BASE (S)	248 Wh kg^{-1}	60
2015 Li et al. (2015a)	Na-$FeCl_2$	190	BASE (S)	135 Wh kg^{-1}	100
2017 Chang et al. (2017)	Na-$NiCl_2$	190	BASE (S)	133 Wh kg^{-1}	150
2017 Ao et al. (2017a)	Na-S/$NiCl_2$	300	BASE (S)	449 Wh kg^{-1*}	50
2018 Chang et al. (2018a)	Na-$NiCl_2$	190	BASE (S)	405 Wh kg^{-1}	300
2019 Ahn et al. (2019)	Na-$NiCl_2$/$FeCl_2$	300	BASE (S)	579 Wh kg^{-1*}	100
2020 Gao et al. (2020)	Na-$NiCl_2$	190	BASE (S)	405 Wh kg^{-1*}	400
2020 Zhan et al. (2020a)	Na-$FeCl_2$	190	BASE (S)	295 Wh kg^{-1}	200
2020 Li et al. (2020a)	Na-$NiCl_2$	190	BASE (S)	263 Wh kg^{-1}	170
2023 Lan et al. (2023)	Na-$NiCl_2$/$FeCl_2$	300	BASE (S)	300 Wh kg^{-1}	60
2007 Parthasarathy et al. (2007)	Na-$ZnCl_2$	400	BASE (S)		
2018 Lu et al. (2018)	Na-$ZnCl_2$	190	BASE (S)		45
2019 Niu et al. (2019)	Na-$CuCl_2$	175	BASE (S)	375 Wh kg^{-1}	50
2021 Niu et al. (2021)	Na-$CuCl_2$	175	BASE/IL (S/L)	322 Wh kg^{-1*}	20
2023 Heinz et al. (2023)	Na-$ZnCl_2$	280	BASE (S)	231 Wh kg^{-1}	22
2017 Small et al. (2017)	Na-I	150	NaSICON (S)	150 Wh kg^{-1}	250
2017 Xue et al. (2017)	Na-$NaAl_2Cl_7$	200	NaSICON (S)	366 Wh kg^{-1}	7
2020 Gross et al. (2020a)	Na-I	110	NaSICON (S)	167.5 Wh L^{-1}	200
2020 Zhan et al. (2020b)	Na-$NaAlCl_4$	190	BASE (S)	447 Wh kg^{-1}	200
2021 Gross et al. (2021)	Na-I	110	NaSICON (S)	223 Wh L^{-1}	400
2023 Weller et al. (2023)	Na-$NaAl_2Cl_7$	190	BASE/NaSICON (S)	194 Wh kg^{-1}	345
2015 Spatocco et al. (2015)	Na-(Pb-Bi)	270	NaOH-NaI (MS)	148 Wh kg^{-1*}	100
2016 Xu et al. (2016)	Na-Zn	560	NaCl-$CaCl_2$ (MS)		40
2020 Ding et al. (2020a)	Na-(Ga-In)	30	$NaClO_4$ in DME/FEC (L)	181 Wh L^{-1}	100
2020 Ding et al. (2020b)	Na-(Bi-Sn-In)	100	NaI in tetraglyme (L)	302 Wh kg^{-1*}	40
2022 Zhou et al. (2022)	Na-Bi_9Sb	450	LiCl-NaCl-KCl (MS)	143 Wh kg^{-1*}	700
2015 Shamie et al. (2015)	Na-V (NFB)	25	BASE (S)	132 Wh kg^{-1*}	5
2016 Liu et al. (2016)	Na-V (NFB)	25	BASE (S)	126 Wh kg^{-1*}	30
2017 Holzapfel et al. (2017)	Na-I (NFB)	100	NaSICON (S)	228 Wh kg^{-1}	20
2018 Yang et al. (2018)	Na-S (NFB)	100	BASE (S)	484 Wh kg^{-1*}	55
2022 Flynn et al. (2022)	Na-S (NFB)	125	NaSICON (S)	210 Wh L^{-1}	170
2021 Wang et al. (2021)	Na-S	150	BASE/IL (S/L)	457 Wh kg^{-1*}	1,000

BASE, β"-Alumina Solid Electrolyte; IL, ionic liquid; NFB, Na flow battery; DME, dimethoxyethane; FEC, fluoroethylene carbonate.

In these next-generation batteries, particular interest has been paid to improving positive electrode performance and developing effective solid electrolytes (and often, coatings) to regulate the sodium|electrolyte interface. This section will highlight recent works dedicated to developing these next-generation molten Na batteries. Generalized schematics of the battery technologies covered in this section are shown in Figure 4.

3.1 Lower-temperature molten sodium batteries

3.1.1 ZEBRA-style batteries

As stated previously, the $NaAlCl_4$ catholyte in ZEBRA batteries liquefies near 154°C. Na metal is molten at temperatures above 98°C. This means that, theoretically, ZEBRA batteries could be operated at

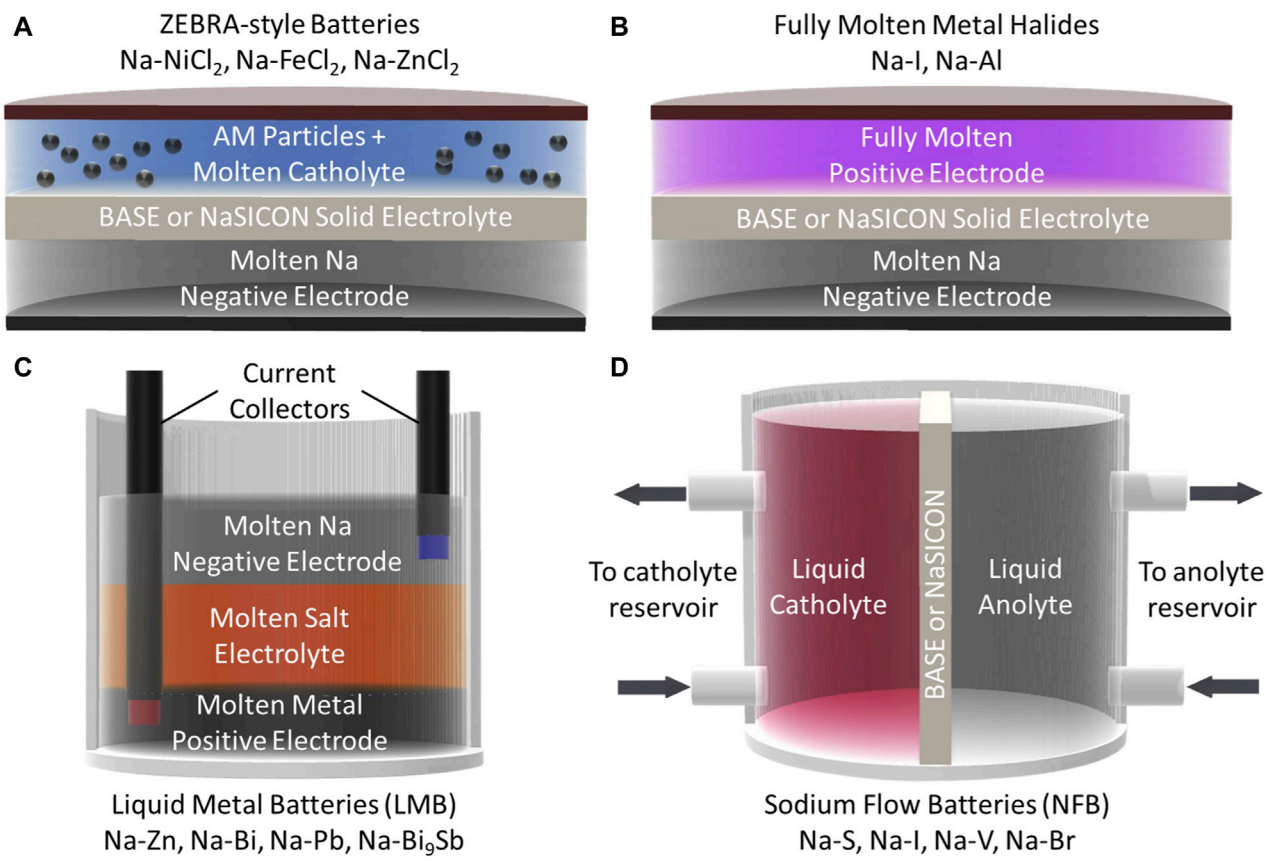

FIGURE 4
Schematics of **(A)** ZEBRA-style molten sodium batteries (AM = active material), **(B)** fully molten metal halide batteries, **(C)** liquid metal batteries (LMB), and **(D)** sodium flow batteries (NFB).

temperatures as low as 154°C and still maintain the benefits of a liquid catholyte and negative electrode. Namely, these benefits are higher conductivity of active Na^+ ions and improved contact at the catholyte|electrolyte interface (a liquid|solid interface as opposed to a solid|solid interface) (Gerovasili et al., 2014; Lu et al., 2014; Li et al., 2016a). However, in practice, it is difficult to decrease the temperature to 154°C. The difficulties can be attributed to the increased catholyte viscosity and decreased Na^+ conductivity in both the catholyte and solid electrolyte. In the classical tubular configuration, temperatures down to 240°C have been studied by Gerovasili et al. (2014) Interestingly, at these reduced temperatures, the solid salt particles ($NiCl_2$ and particularly NaCl) maintain a smaller average particle size compared to operation at higher temperatures. This is beneficial as the smaller particles provide more active surface area for the electrochemical reactions to proceed, leading to less polarization. These findings would point to lower temperatures as preferable for ZEBRA battery operation, but they are limited to ~240°C in the tubular configuration due to the reduced catholyte conductivity at that temperature (Gerovasili et al., 2014).

To take advantage of the benefits at temperatures below 240°C, planar configurations of the ZEBRA battery have been proposed (Lu et al., 2012; Li et al., 2014; Lu et al., 2017). A planar ZEBRA-style battery configuration is illustrated in Figure 4A. The thinner electrodes used in planar designs shorten diffusion pathways and increase active surface area to lessen the effect of lower conductivity in the positive electrode. A planar design also allows for the use of thinner electrolytes (which can improve energy and power density) and facilitates easier cell packing and thermal regulation. In 2016, Li *et al.* demonstrated a planar Na-$NiCl_2$ battery that operated as low as 190°C with an energy density of 350 Wh kg^{-1} and a lifetime of over 1,000 cycles (Li et al., 2016a). The improved energy density was attributed to the planar design and the lower temperature slowed particle growth, leading to a long cycle life. Further, reducing excess Ni content in the positive electrode can boost energy density, both reducing cost and enhancing performance (Li et al., 2013; Li et al., 2016a; Chang et al., 2018a). Planar ZEBRA-style cells have also been operated near 300°C to reduce electrolyte resistance and enable high current densities up to 80 mA cm^{-2}. (Lan et al., 2023).

To further enhance the performance of Na-$NiCl_2$ cells, various cathode architectures have been proposed. Positive electrodes composed of carbon fibers with dispersed Ni particles can maintain a conductive network and constrain particle growth during cycling (Li et al., 2020a; Gao et al., 2020). Li *et al.* showed that $NiCl_2$/graphene aerogel positive electrodes with high electronic conductivity exhibited low polarization and allowed for the reduction of excess Ni (Li et al., 2021a). Ni-coated graphite particles introduced by Chang *et al.* provided robust conductive pathways in the electrode, whilst also eliminating a portion of electrochemically inactive Ni (Chang et al., 2017). Encapsulating

Ni particles within a Ni_3S_2 shell was shown to mitigate particle growth and enhance cycle life of Na-$NiCl_2$ cells (Ao et al., 2017a; Ao et al., 2017b). These studies generally suggest that architectures capable of limiting Ni particle growth can effectively improve the performance of Na-$NiCl_2$ cells (Kim et al., 2017; Ahn et al., 2019).

Additional reports have shown that costs can be reduced by partially or completely eliminating Ni from the positive electrode. Lu *et al.* showed that a combination Na-S/$NiCl_2$ battery could operate with capacity contribution from both active materials (Lu et al., 2013a). $FeCl_2$ is a common additive to $NiCl_2$ positive electrodes in ZEBRA cells, but positive electrodes using purely $FeCl_2$ have also been reported and completely eliminate the supply risk of Ni (Li et al., 2015a; Zhan et al., 2020a; Frusteri et al., 2022). These lower-cost batteries may sacrifice some energy density (295 Wh kg^{-1}) to reduce positive electrode material costs by ~94% (1.95 \$ kWh^{-1} for $FeCl_2$ vs. 31.78 \$ kWh for $NiCl_2$) (Li et al., 2015a; Zhan et al., 2020a).

3.1.2 Metal chlorides beyond $NiCl_2$ and $FeCl_2$

Other metal chlorides can be substituted for $NiCl_2$ and $FeCl_2$ in molten sodium batteries. Parthasarathy et al. (2007) proposed a high-temperature (400°C) Na-$ZnCl_2$ that used a $ZnCl_2$/NaCl catholyte and benefited from lower-cost and non-corrosive $ZnCl_2$. The cell relied on the overall reaction (Eq. 8):

$$2Na\,(l) + ZnCl_2\,(s\,or\,l) \leftrightarrow 2NaCl\,(s) + Zn\,(s) \tag{8}$$

and provided a discharge voltage of ~2.0 V. Researchers have since tried to lower the operating temperature of Na-$ZnCl_2$ cells to further reduce costs. Lu *et al.* used the traditional $NaAlCl_4$ catholyte to reduce the temperature to 280 °C. Zn and NaCl particle growth was limited at this temperature which helped maintain cell reversibility (Lu et al., 2013c) The same group eventually lowered the temperature even further to 190°C and proposed the following two-step reaction mechanism (Eqs 9, 10):

$$4NaCl\,(s) + Zn\,(s) \leftrightarrow Na_2ZnCl_4\,(s) + 2Na\,(l) \tag{9}$$

$$Na_2ZnCl_4\,(s) + Zn\,(s) \leftrightarrow 2ZnCl_2\,(s) + 2Na\,(l) \tag{10}$$

that provided discharge voltages of 1.94 and 2.13 V, respectively (Lu et al., 2018) Similar to $NiCl_2$/$FeCl_2$ batteries, electrode architectures and different NaCl/$ZnCl_2$ ratios have been studied to understand the influence of particle growth on battery performance (Kim et al., 2015b; Lee et al., 2019) This extensive effort has led to the recent demonstration of high capacity (38 Ah) tubular Na-$ZnCl_2$ cells by Heinz *et al.* (from the Solstice project) which benefited from an improved understanding of the $AlCl_3$-NaCl-$ZnCl_2$ secondary electrolyte and precursor morphology (Heinz et al., 2023; Kumar et al., 2023; Solstice, 2023; Sieuw et al., 2024).

In addition to $ZnCl_2$, $CuCl_2$ has been explored as a potential positive electrode material. Niu *et al.* reported a Na-$CuCl_2$ battery that operated at 175°C and relied on a 1-ethyl-3-methylimidazolium bis(trifluoromethylsulfonyl)imide ([EMIM][TFSI]) ionic liquid catholyte. The group also reported similar issues related to particle growth and aggregation during cycling (Niu et al., 2019; Niu et al., 2021).

3.1.3 Fully molten metal halide batteries

The absolute minimum temperature of classical ZEBRA batteries (which use $NiCl_2$ and $FeCl_2$) is the melting point of the $NaAlCl_4$ catholyte, 154°C. However, since Na is molten as low as 98°C, new positive electrode materials have the potential to further reduce temperature while maintaining the benefits of liquid electrodes. In 2017, Small *et al.* introduced a new molten NaMH battery chemistry that could be operated down to 120°C that relied on the electrochemical couple of Na and iodide (Small et al., 2017). This lower temperature was enabled by using a NaI-$AlCl_3$ positive electrode. A 50:50 (atomic %) mixture of these salts has a melting point near 95°C, even lower than that of Na metal, unlocking a new temperature regime for molten Na batteries. This fully molten design is illustrated in Figure 4B. The elements in these electrodes are abundant (Al is the second most abundant element in the Earth's crust) and, along with the temperature decrease, provide the opportunity for significant cost reduction for grid-scale storage (Small et al., 2017). As opposed to many of the metal-chloride batteries that used BASE, the NaI batteries used the Na Super Ionic CONductor (NaSICON) as the solid electrolyte, with the formula $Na_{1+x}Zr_2Si_xP_{3-x}O_{12}$ (with $0 \le x \le 3$) (Goodenough et al., 1976). NaSICON was selected for this chemistry due to improved conductivity at moderate temperatures, allowing higher current densities to be passed through the batteries below 150°C (Small et al., 2017). NaSICON will be discussed in more detail in a following section.

The ideal positive half-cell and overall reactions are listed in Eqs 11, 12. Note that this chemistry still employs a molten Na negative electrode with the same half-cell reaction as shown in Eq. 1.

$$I_3^- + 2e^- \rightarrow 3I^- \tag{11}$$

$$2Na + I_3^- \rightarrow 2Na^+ + 3I^- \tag{12}$$

This reaction would provide a theoretical voltage of 3.24 V, higher than Na-S or the previous metal chloride batteries. In practice, the reported batteries showed voltages just below 3 V due to various polarization sources. The elevated voltage and high concentration of redox-active I^- in the molten salt allow for an energy density of 150 Wh kg^{-1}, slightly higher than the traditional ZEBRA chemistry. These batteries were capable of cycling under various conditions for >3,000 h, with the added benefit that the electrode materials could be cooled, solidified, and reheated to their liquid state without adverse affecting performance. The ability to reversibly freeze and melt the active materials means that these batteries could survive harsh conditions even if their thermal regulation failed, which is extremely important for resilient storage. Further, this new chemistry was shown to be extremely safe, with negligible gas formation and only benign products (e.g., Al, NaI and NaCl) formed upon mixture of the positive and negative active materials (Small et al., 2017).

The Na-I batteries could be optimized to reduce the temperature even further. Gross *et al.* reported that if NaI-$AlBr_3$ was used as the positive electrode instead of NaI-$AlCl_3$, the batteries could be operated down to 110°C (Gross et al., 2020a). However, the new positive electrode suffered from significantly slower redox kinetics that limited high-current applications. Reaction kinetics could be improved by using a NaI-$GaCl_3$ positive electrode that was found to operate similarly to $AlCl_3$ and even elevated the nominal cell voltage to an impressive 3.65 V (Lee et al., 2021; Percival et al., 2021). The increased voltage was attributed to the complexation environment of I^- and I_3^- in the $GaCl_3$ and provides a pathway for even higher energy

density molten sodium batteries (Gross et al., 2021). Optimization principles learned from the NaI-$GaCl_3$ system eventually enabled 110°C operation of the original NaI-$AlCl_3$ chemistry (Maraschky et al., 2023a; Maraschky et al., 2023b). Detailed studies of catholyte phase diagrams, reaction pathways, and NaSICON/catholyte/current collector interfaces show promise towards enabling these fully molten NaMH batteries (Percival et al., 2018; Lee et al., 2021; Maraschky et al., 2023a; Maraschky et al., 2023b).

Fully molten Na-Al batteries can also be fabricated using purely molten sodium chloroaluminate as the catholyte (the same catholyte from ZEBRA batteries without any $NiCl_2$ or $FeCl_2$ particles). The trivalent aluminum should provide excellent energy density according to Eq. 13:

$$3Na + AlCl_3 \leftrightarrow 3NaCl + Al \tag{13}$$

which has a theoretical potential of 1.8 V. Xue *et al.* used $NaAl_2Cl_7$ as a catholyte and achieved 366 Wh kg^{-1} with limited cyclability. (Xue et al., 2017) Other groups opted for the basic $NaAlCl_4$ catholyte, which could benefit from a simpler one-step conversion reaction and less corrosivity than the acidic $NaAl_2Cl_7$, and showed an extremely high energy density of 447 Wh kg^{-1} over 200 cycles (Zhan et al., 2020b) The acidic $NaAl_2Cl_7$ melt continues to be of particular interest, though, due to its higher theoretical energy density (~493 Wh kg^{-1}) (Weller et al., 2023) Fully molten NaMH batteries mitigate the concerns of particle ripening and disconnection that plague their ZEBRA counterparts and are an intriguing option for long-life, high-current molten Na batteries.

3.1.4 Molten sodium batteries beyond metal halide

The potential of molten Na batteries for grid-scale storage has motivated the development of many chemistries beyond metal halides. Liquid metal batteries (LMBs) are one example of these molten Na chemistries. These batteries contain two fully molten metallic electrodes and a molten salt electrolyte. The three molten layers naturally separate due to density differences to avoid short-circuiting as shown in Figure 4C; (Kim et al., 2013). Though the first LMBs can be traced back to 1960, the chemistry has regained attention for grid storage recently (Bernard, 1960; Crouthamel and Recht, 1967; Kim et al., 2013; Li et al., 2016b). Bi, Pb, Sn, Sb, Ga, In, Zn, and various other metals have been considered potential positive electrodes. (Kim et al., 2013). In 2016, Xu *et al.* reported a Na-Zn LMB that operated at 560 °C and combined molten Na and Zn electrodes with a NaCl-$CaCl_2$ molten salt electrolyte (Xu et al., 2016). Spatocco *et al.* demonstrated that lower-temperature (270°C) Na-LMBs were possible when they reported a Na-(Pb-Bi) battery with a NaOH-NaI molten salt electrolyte (Spatocco et al., 2015). One prominent issue with Na-based LMBs has been the solubility of Na in the molten salt electrolytes, leading to relatively high self-discharge rates. In 2022, Zhou *et al.* reported a multi-cationic electrolyte of LiCl-NaCl-KCl that had limited Na solubility leading to smaller rates of self-discharge and stability over 700 cycles (Zhou et al., 2022). More details regarding molten salt electrolytes will be discussed in a subsequent section.

Anoterh strategy to improve Na-LMBs is to lower the temperature even further in order to use more traditional organic electrolytes. This has been demonstrated by Ding *et al.* in a Na-(Ga-In) battery operated at 30°C that used a $NaClO_4$ in dimethoxyethane/fluoroethylene carbonate electrolyte. A Na-K alloy was used as the negative electrode to maintain all-molten electrodes at this low temperature (Ding et al., 2020a). The same group also reported a Na-(Bi-Sn-In) LMB at 100°C with a NaI in tetraglyme electrolyte that eliminated the use of costly Ga and In (Ding et al., 2020b). The low operating voltage (<2 V) of LMBs may somewhat limit their applicability, but their low cost, high capacity, and high reversibility are promising for grid-scale storage.

Metal-air batteries have potential as high energy density storage systems, due to the compact and lightweight carbon cathodes that mediate oxygen electrochemistry. While research has been limited, molten Na-air batteries were first explored by Peled *et al.*, who used carbon- and cobalt oxide-based positive electrodes coupled with a polyethylene oxide (PEO) + NaTf electrolyte at 105°C (Peled et al., 2013). The electrolyte showed a wide voltage window, and the batteries exhibited good cyclability, but sluggish oxygen electrochemistry resulted in low current densities. Recently, Zhu *et al.* demonstrated a molten Na-air battery that used Ni powder mixed with a $NaNO_3$ + KNO_3 + $CsNO_3$ eutectic molten salt as the positive electrode (Zhu et al., 2022b). The group showed that the nitrate anions in the molten salt mediated an overall $2e^-/O_2$ reaction that formed Na_2O_2 as the final discharge product. Full cells could be cycled 400 times with a capacity of 0.5 mA h cm^{-2} at 5 mA cm^{-2}. Further improvement and understanding of oxygen electrochemistry will be vital to further advancing molten Na-air batteries.

Another emerging chemistry is that of molten Na flow batteries (NFBs). The concept of NFBs was proposed by Shamie *et al.* using a Na-V redox couple as an example and is illustrated in Figure 4D. The batteries would be operated in the same fashion as conventional flow batteries, with a liquid catholyte and molten sodium as the anolyte being pumped from a large reservoir into an electrochemical cell. They suggested that a traditional vanadium redox-flow catholyte could be cycled between V^{3+} and V^{5+} to attain a high theoretical specific energy of ~355 Wh kg^{-1} (Shamie et al., 2015). The group later demonstrated this concept using a Na-Cs alloy (molten at RT) coupled with a BASE separator and V-based aqueous catholyte, and the cell retained >99% of its original capacity over 30 cycles (Liu et al., 2016). However, the cost limitations of V-based NFBs has motivated research into other redox couples. NFBs using aqueous bromine and iodine catholytes have been reported by Holzapfel *et al.* and were able to achieve energy densities near 200 Wh kg^{-1} (Holzapfel et al., 2017; Gerbig et al., 2023). While room-temperature molten alloys (Na-K and Na-Cs) are intriguing materials for molten Na batteries, they react aggressively with air and moisture (even more so than pure Na metal) and significant engineering controls will be necessary to successfully implement them in LMBs, especially if they are paired with an aqueous catholyte.

The original Na-S chemistry has also been adapted to a NFB by various groups. The Na-S NFBs still use molten Na negative electrodes and a solid electrolyte of BASE or NaSICON but utilize S sources that can be converted to flow-type batteries. Yang *et al.* used a suspension of S and C particles in a 1 M NaI tetraglyme solution as a catholyte to achieve a Na-S NFB that maintained a capacity of 484 mA h g^{-1} after 55 cycles. Flynn *et al.* instead used sodium polysulfide (Na_2S_x) dissolved in an organic solvent to fabricate an NFB capable of 170 cycles with a

specific energy of 210 Wh/L at ~120°C (Flynn et al., 2022). The technology described by Flynn *et al* is being further developed by Enlighten Innovations and is in the advanced stages of precommercial development (Enlighten, 2023). The ability to decouple energy and power in NFBs could prove vital to addressing the diverse demands of grid-scale energy storage. Finally, though details are outside the scope of this review, it is worthwhile to mention that room temperature Na-S batteries have been explored but are yet to be commercialized, as they are often plagued by the electrochemical irreversibility of solid polysulfide compounds or soluble polysulfide shuttling in aqueous electrolytes (Kim et al., 2016; Wei et al., 2016; Gross and Manthiram, 2019; Wang et al., 2020a; Wang et al., 2020b). A summary of various molten Na-based battery research reports is provided in Table 2. The authors believe it important to emphasize that these research reports do not represent the commercial performance of molten Na batteries, which have much longer cycle lives (1,000 s of cycles).

3.2 Electrolytes for molten sodium batteries

3.2.1 β″-alumina solid electrolyte (BASE)

BASE was initially thought to be a polymorph of Al_2O_3, but, in the early 1900s, Pauling showed that the structure contained sodium (Pauling, 1927). In 1967, Yao and Kummer of the Ford Motor Company first reported fast ion conduction in BASE, which was instrumental in the development of the first Na-S battery in the late 1960s. Since then, BASE has been used widely in both Na-S and ZEBRA batteries and has even found use in several all-solid-state battery (ASSB) technologies (Wenzel et al., 2016; Bay et al., 2020; Fertig et al., 2022; Fertig et al., 2023).

Beta aluminum oxides are comprised of alternating closely-packed layers and loosely-packed layers. The closely-packed layers serve as structural layers that consist of four layers of oxygen ions that contain aluminum (Al) ions in tetrahedral and octahedral interstitial sites. The loosely-packed layers contain mobile Na ions that can be driven under the influence of an electric field. The mobile Na provides the conductivity necessary to make useful solid electrolytes. There are two crystal structures of beta alumina oxides–β-Al_2O_3 and β″-Al_2O_3. The two structures have slightly different stoichiometries, stacking sequences, and Na occupation. Na diffuses through two sites in beta alumina, the Beevers-Ross and anti-Beevers-Ross sites. Only the Beevers-Ross site is occupied in the β form, while both are occupied in the β″ form. In short, the β″-Al_2O_3 form (which will continue to be referred to as BASE) has more mobile Na, raising its conductivity and making it the preferred phase for solid electrolytes. The structures of both forms are shown in Figure 5; (Chi et al., 2017). Typical polycrystalline BASE has a conductivity near 200 mS cm^{-1} at 300°C (Beevers and Ross, 1937; Yung-Fang Yu and Kummer, 1967; Kummer, 1972; Kim et al., 1979; Dell and Moseley, 1981; Engstrom et al., 1981; Almond et al., 1982; Lu et al., 2010a; Lu et al., 2010b).

The properties of BASE can be manipulated through careful control of its composition and processing parameters. Several authors have shown that aliovalent doping of the Al^{3+} sites in the structural layers with magnesium (Mg^{2+}) or lithium (Li^{+}) leads to excess negative charge that can be balanced by additional mobile Na^{+} ions (Bates et al., 1981; Lee et al., 2017; Dirksen et al., 2021). BASE is fabricated through solid-state reaction, sol-gel processes, or co-precipitation (Ray and Subbarao, 1975; Choy et al., 1993; van Zyl et al., 1993; Certo et al., 1998; Park et al., 2005; Mali and Petric, 2012; Barison et al., 2015). These methods all rely on first synthesizing BASE in its powder form and then sintering to attain the final desired shape. The sintering process can impact many characteristics of BASE such as phase purity and microstructure. The low-conductivity β phase is difficult to fully eliminate during synthesis, leading to different conductivities depending on phase purity (Youngblood et al., 1978; Stevens and Binner, 1984). Interestingly, the pure β″ phase is susceptible to mechanical weakness and moisture sensitivity, making slight β phase, ZrO_2, or YSZ inclusions desirable in practice (Virkar, 2008; Lu et al., 2010b; Lu et al., 2015; Li et al., 2019). Grain growth during sintering is affected by both sintering time and temperature. Larger grains lead to higher overall conductivity, due to less high-resistance grain boundaries interfering with Na^{+} transport. High sintering temperatures (which are often >1,500°C) can lead to sodium evaporation and compositional changes. (Lu et al., 2010b).

Multiple advanced techniques are being explored to further improve the manufacturing and microstructure of BASE. Spark plasma sintering (SPS) is a promising processing technique that uses pulsed AC or DC current to rapidly heat a compressed powder and can lower sintering times from many hours to mere minutes. Koganei *et al.* showed that 98% dense BASE could be obtained using SPS by heating under compression to 1,400°C (100°C min^{-1}), holding for 15 min, and allowing the pellets to cool naturally. The quick temperature ramp and short hold time can significantly reduce the cost of heating to such high temperatures and also minimize the volatilization of sodium, leading to lower cost, enhanced compositional control, and, critically, an extremely high room-temperature conductivity of 19 mS cm^{-1} (Koganei et al., 2014). Li *et al.* used lower-temperature (1,300°C) SPS to obtain >96% dense BASE with a conductivity of 183 mS cm^{-1} at 350°C (Li et al., 2020b). Freeze drying before SPS and high-temperature sintering after SPS have also been shown to produce mechanically strong, highly conductive (239 mS cm^{-1} at 350°C), but the high-temperature step negates some of the benefits of pure SPS processing (Li et al., 2021b). All groups attributed the high (and anisotropic) conductivities to highly c-axis oriented BASE. Similarly, microwave-assisted sintering has been preliminarily investigated and produced 86% dense BASE by applying 2,450 MHz microwaves during a 40 min hold at 1,300°C. (Mortalò et al., 2020).

Cold sintering also has the potential to lower the cost of fabricating BASE. Cold sintering uses a transient secondary phase to assist in obtaining the desired phase. Briefly, the electrolyte powder is mixed in an aqueous solution or with a (relatively) low melting point material (such as NaOH) and heated. At elevated temperatures, the transient liquid phase can promote densification at lower temperatures before evaporating or extruding from the die. For example, Grady *et al.* showed that >92% dense BASE could be obtained at 375 °C using a transient fused NaOH solvent. The BASE pellets exhibited a conductivity of 10 mS cm^{-1} at 300°C, which could be improved by heating the pellets to 1,000°C (Grady et al., 2021). Optimizing sintering parameters, particularly by minimizing time and/or temperature, remains as the most practical pathway for

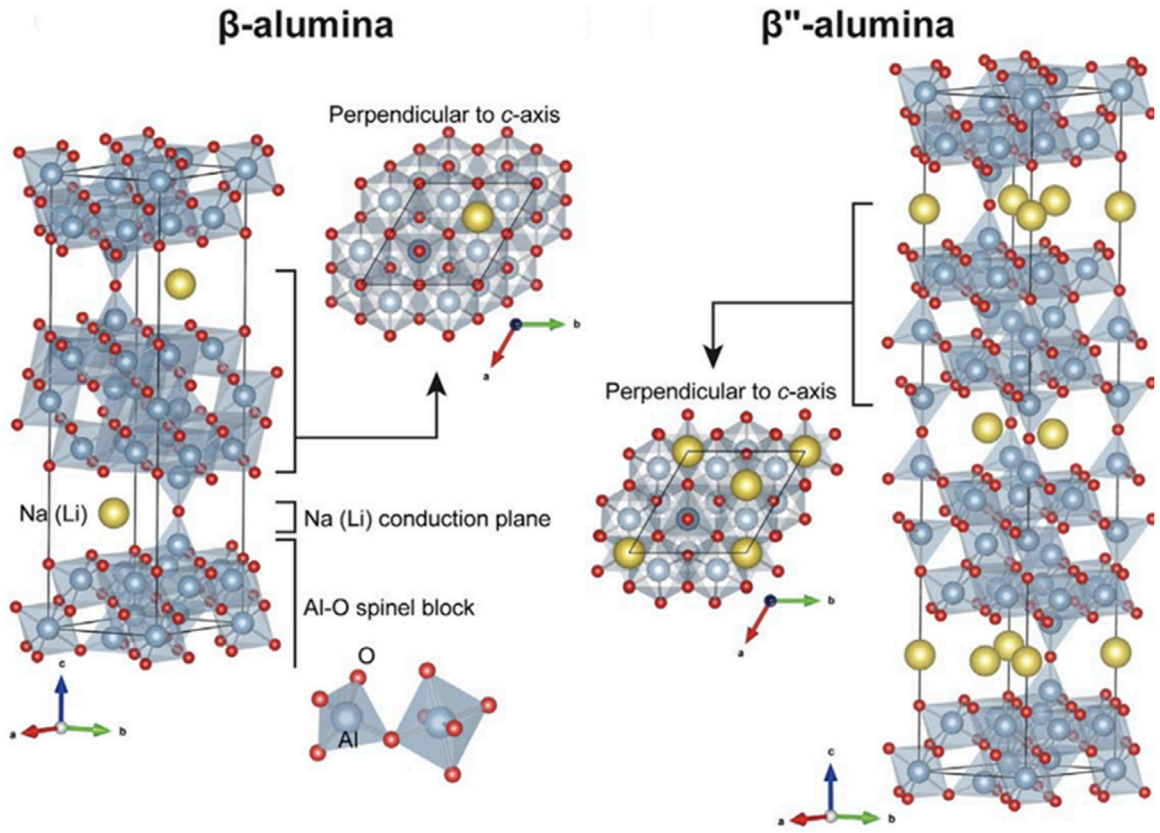

FIGURE 5
Structures of Na β-alumina and Na β¨-alumina. Reproduced with permission from Ref. 137. Copyright 2017, Elsevier.

reducing BASE (and thereby molten Na battery) costs and efforts in this field should be prioritized.

3.2.2 Na Super Ionic CONductor (NaSICON)

NaSICON is an oxide ceramic with the formula $Na_{1+x}Zr_2Si_xP_{3-x}O_{12}$, $0 \leq x \leq 3$, that was reported by Hong and Goodenough in 1976 (Goodenough et al., 1976). NaSICON is a solid solution of $NaZr_2P_3O_{12}$ and $Na_4Zr_2Si_3O_{12}$ and has a rhombohedral structure ($R\bar{3}c$), except within the range $1.8 \leq x \leq 2.2$ where a monoclinic distortion (C2/c) is observed below 150°C. The solid solution creates a three-dimensional framework consisting of ZrO_6 octahedra that share corners with SiO_4 or PO_4 tetrahedra. This framework contains "bottlenecks" that sodium ions can move through, jumping between sites to provide Na^+ conductivity (Goodenough et al., 1976; Boilot et al., 1987; Rajagopalan et al., 2021). Specifically, there are three sites that Na can occupy in the monoclinic NaSICON structure, named Na(1), Na(2), and Na(3). The Na(1) and Na(2) sites are sixfold coordinated to the oxygen ions of three SiO_4 or PO_4 tetrahedra and are also present in the rhombohedral structure. The Na(3) positions are unique to the monoclinic phase and are threefold coordinated to the oxygen ions of three ZrO_6 octahedra. These Na sites are only partially filled (with the extent depending on stoichiometry) and Na^+ hops between occupied and vacant sites to provide conductivity. Briefly, the additional Na sites present in the monoclinic phase ($1.8 \leq x \leq 2.2$) provide the highest conductivity (near 200 mS cm^{-1} at 300°C) in the compositional range and make it the preferred stoichiometry for solid electrolyte applications (Kohler et al., 1983; Kohler and Schulz, 1985; Boilot et al., 1988; Guin and Tietz, 2015). The structure of NaSICON is illustrated in Figure 6.

Since its discovery, NaSICON has been proposed as a replacement for BASE due to its excellent Na^+ conductivity, particularly at lower temperature, as well as its environmental insensitivity, and its ease of machineability. The conductivity at lower temperatures makes it a particularly useful electrolyte as molten Na batteries push towards operating temperatures below 200 °C. Using the nominal NaSICON composition, $Na_3Zr_2Si_2PO_4$, Small *et al.* reported a NaSICON conductivity of 140 mS cm^{-1} at 200°C, slightly higher than BASE at the same temperature. NaSICON's excellent low-temperature conductivity became more evident at room temperature, where its conductivity (>1 mS cm^{-1}) was quite higher than BASE (Small et al., 2017). The improved conductivity at lower temperatures is thought to be, at least partially, a result of the three-dimensional NaSICON framework, as opposed to relying on two-dimensional conduction planes in BASE (Goodenough et al., 1976; Kohler et al., 1983; Kohler and Schulz, 1985; Boilot et al., 1988; Guin and Tietz, 2015; Small et al., 2017). Furthermore, aliovalent doping of the Zr site in NaSICON can raise the room-temperature conductivity even higher to above 2 mS cm^{-1}. (Jolley et al., 2015a). Like BASE, doping the Zr^{4+} site with lower valent cations, such as Al, Y, Fe, Co., Ni, or Zn, results in an increased concentration of Na^+ ions to achieve charge neutrality (Jolley et al., 2015b; Samiee et al., 2017). Grain size and presence of

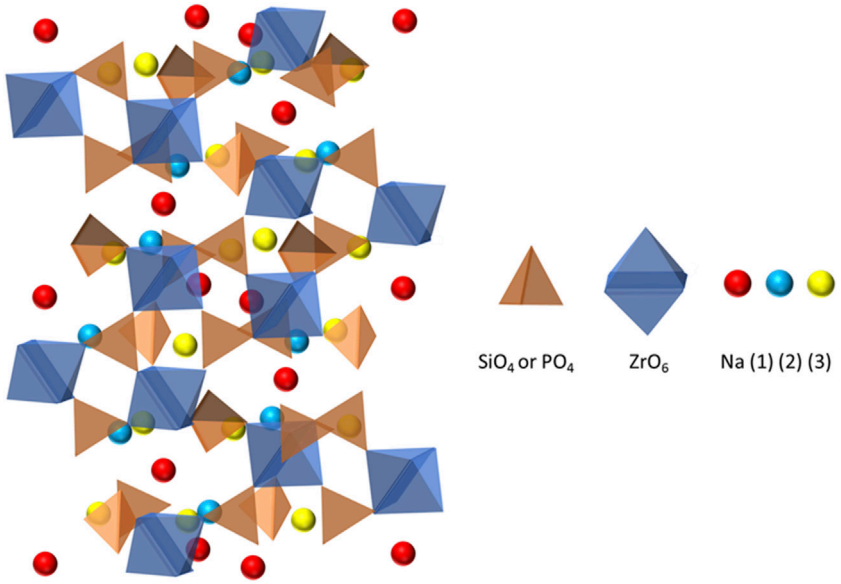

FIGURE 6
Structure of NaSICON showing interconnected silicate/phosphate tetrahedra and zirconia octahedra.

grain boundaries also influence the ionic conductivity, with larger grains typically leading to higher total conductivities (Fuentes et al., 2001; Nieto-Muñoz et al., 2020).

Many similar manufacturing techniques used for BASE have been successfully applied to NaSICON. However, NaSICON has one critical processing advantage compared to BASE. NaSICON can traditionally be sintered at much lower temperatures (~1,100°C–1,200°C) with mostly complete conversion to the desired phase and high density (Goodenough et al., 1976; Gross et al., 2020b). This is much lower than the 1,450°C typically necessary for BASE and can significantly lower production costs (Ray and Subbarao, 1975; Liu et al., 2020). This is vitally important as the solid electrolyte is often viewed as one of the costlier components in molten Na batteries, often due to their high sintering temperatures (Lu et al., 2010b; Lu et al., 2013c). Liquid phase sintering using additives such as Bi_2O_3, Na_2SiO_3, or Na_3BO_3 enables sintering temperatures as low as 900°C and can reduce densification times due to enhanced liquid-state diffusion (Noi et al., 2018; Suzuki et al., 2018; Oh et al., 2019; Miao et al., 2021). Sol gel-processing, which dates back to the 1980s, can bring processing temperatures to ~700°C. (Shimizu et al., 1997; Zhang et al., 2004; Bell et al., 2014). Fused hydroxide cold sintering at 375°C by Grady *et al.* achieved 93% dense NaSICON with a room-temperature conductivity of 0.2 mS cm^{-1}. (Grady et al., 2020). A recent patent using the fused hydroxide cold sintering method reported 89% densification of NaSICON at just 150°C, but this lower density resulted in a conductivity of 1.13 x 10^{-5} mS cm^{-1} at 35°C. (Bock et al., 2023). Aqueous transient phases can push the cold sintering temperature even lower, as demonstrated by Leng *et al.*, who showed that 83% dense Mg-doped NaSICON could be obtained by cold sintering at 140°C. However, a second annealing step at 1,100°C was necessary to achieve a room-temperature conductivity of 1.36 mS cm^{-1}. (Leng et al., 2018). This method was further explored by combining cold sintering with liquid phase sintering using a Bi_2O_3 additive that melted near 820°C and helped increase the final conductivity >1.5 mS cm^{-1} (Leng et al., 2019). Room temperature fabrication of thin NaSICON films (3.5–10 μ m) via powder aerosol deposition (PAD) was reported by Sozak *et al.* PAD relies on accelerating powder particles, colliding them with a substrate, and converting kinetic energy to bonding energy to build a dense film. The PAD method produced NaSICON with room-temperature conductivity of just 1.5 μ S cm^{-1} (after annealing at 600 °C), but the ability to make thin films could combat some of the conductivity loss (Sozak et al., 2023). Economical, large-scale synthesis of highly-conductive and mechanically robust NaSICON will be critical towards commercialization and widespread adoption of lower-temperature molten Na batteries.

One concern with the use of NaSICON for Na batteries is the chemical compatibility with Na metal. Early studies presented theoretical and experimental evidence that NaSICON was unstable in the presence of Na metal (Schmid et al., 1982; Tsai and Hong, 1983). These were mainly focused on using NaSICON as an electrolyte for Na-S batteries, and experimental studies were accordingly carried out near 300°C. Discoloration, lattice parameter changes, and fracturing were observed after immersing NaSICON in molten Na metal for extended periods of time. These changes indicated reaction with Na, which would have increased the Na content of NaSICON and subsequently caused stresses in the electrolytes, leading to fracture (Kreuer and Warhus, 1986). Further studies suggested that these degradation pathways were kinetically dominated, meaning that stable performance at lower temperatures could be possible (Warhus et al., 1988; Zhang et al., 2020a). Accordingly, Zhou *et al.*, from the Goodenough group, showed that NaSICON was chemically stable in the presence of Na metal up to at least 175°C. As predicted, at temperatures above 300°C, NaSICON could be partially reduced and amorphized upon reaction with Na, but this actually improved molten Na wetting (Zhou et al., 2017). The low-temperature stability and non-

catastrophic pathways at elevated temperatures imply that NaSICON can be used without significant risk of chemical decomposition in long-lifetime molten Na batteries.

3.2.3 Glass and glass-ceramic conductors

While BASE and NaSICON have traditionally been the primary electrolyte options for molten Na batteries, other Na^+-conducting materials have been proposed as potential electrolytes. Borate, aluminosilicate, and NaSICON-glass (NASIGLAS) electrolytes were explored in early Na-S cells, but BASE was ultimately favored for its higher conductivity and corrosion resistance (Susman et al., 1983; Herczog, 1985; Bloom et al., 1986; Sudworth and Tilley, 1986). The low-cost materials and processing (typically at lower temperatures) has helped retain interest in glass electrolytes. Braga *et al.* prepared amorphous $A_{2.99}M_{0.005}OCl_{1-z}(OH)_x$ (A = Li or Na, M = Ba or Ca) electrolytes at just 230°C–250°C with room-temperature conductivities >10 mS cm^{-1}. (Braga et al., 2016). Reports of sulfide (Na_3BS_3, Na_2S-GeS_2, Na_2S-P_2S_5, Na_2S-GeS_2-P_2S_5), oxide ($Na_{2.8}Ca_{0.1}Al_2Ga_{0.5}P_{2.7}O_{12}$, Na_2O-Al_2O_3-P_2O_5-Nb_2O_5, $Na_3Al_{1.8}Si_{1.65}P_{1.8}O_{12}$ and $Na_3Al_2P_3O_{12}$), and oxysulfide ($Na_3PS_{4-x}O_x$ and $Na_4P_2S_{7-6x}O_{4.62x}N_{0.92x}$) glasses have also shown room-temperature conductivities >0.1 mS cm^{-1}, and their conductivities often depend strongly on dopant concentrations (Nose et al., 2015; Allu et al., 2018; Keshri et al., 2020; Lazar et al., 2020; Keshri et al., 2021; Tsuji et al., 2021; Chi et al., 2022; Keshri et al., 2022; Nasu et al., 2022; Olson et al., 2023). The elimination of grain boundaries in glass electrolytes is thought of as a distinct advantage over traditional ceramics, as grain boundaries often have reduced conductivity or may act as failure pathways for dendrites.

In addition to the pure glassy electrolytes, glass-ceramic composite electrolytes have recently garnered interest, due to the typically higher conductivity of the ceramic phase. Glass-ceramic composites are often synthesized by fully or partially crystallizing the glassy phase at elevated temperatures. One early example from Hayashi *et al.* is that of Na_3PS_4, where the glassy phase was crystallized to cubic Na_3PS_4 by heating to above 270°C and the resulting electrolyte had a room temperature conductivity of 0.2 mS cm^{-1} (Hayashi et al., 2012; Hayashi et al., 2014; Tatsumisago and Hayashi, 2014). Since then, many glass-ceramic electrolytes have been proposed using the crystallization technique. These also fall into the categories of sulfides (such as Na_3PS_4-Na_4SiS_4, $Na_{2.9375}PS_{3.9375}Cl_{0.0625}$, Na_3PS_4-Na_4GeS_4, Na_3PS_4-NaI, $Na_{10}GeP_2S_{12}$, and $Na_3Si_xSb_{1-x}S_{4-y}Br_y$) and oxides (such as $Na_{1+x}[Sn_xGe_{2-x}(PO_4)_3]$, $Na_{3+x}[Zr_xSc_{2-x}(PO_4)_3]$, $Na_{1+y}Ti_2Si_yP_{3-y}O_{12}$, $(Na_2O + NaF)$–TiO_2–B_2O_3–P_2O_5–ZrF_4, $Na_3Zr_2Si_2PO_{12}$-NaF, $Na_{1+x}Y_yGa_{x-y}Ge_{2-x}(PO_4)_3$, and Na_2O-Y_2O_3-SiO_2) and may exhibit room-temperature conductivities as high as 2.26 mS cm^{-1} ($Na_3Si_xSb_{1-x}S_{4-y}Br_y$), but are typically reported to be near 0.1 mS cm^{-1} (Tanibata et al., 2014; Li et al., 2015b; Hibi et al., 2015; Ni et al., 2015; Chu et al., 2016; Gandi et al., 2018; Manchgesang et al., 2018; Tanibata et al., 2018; Tsuji et al., 2018; Nieto-Muñoz et al., 2019; Shao et al., 2019; Sundar et al., 2019; Gong et al., 2023). Sintered, crystalline thiophosphates with tungsten dopants ($Na_{3-x}Sb_{1-x}W_xS_4$, and $Na_{3-x}P_{1-x}W_xS_4$) can attain even higher room-temperature conductivities, reaching as high as 41 mS cm^{-1} (Hayashi et al., 2019; Fuchs et al., 2020). While these electrolytes show promising Na^+ conductivities, they have not been demonstrated in molten Na batteries. Instead, the studies often showcase their performance in solid-state Na batteries or symmetric cells. The stability of the electrolytes at elevated temperatures and compatibility with molten Na will be important considerations if they are to be applied in molten Na batteries.

3.2.4 Molten salt electrolytes

LMBs were discussed previously and use molten salt electrolytes to separate two molten metallic electrode layers based on density. An 80:20 NaOH-NaI eutectic mixture was shown to have a low melting point of 220 °C, a conductivity of ~500 mS cm^{-1} at 250°C, and was demonstrated for 112 cycles in a Na|NaI-NaOH|Pb-Bi cell. (Spatocco et al., 2015). A 50:50 NaCl-$CaCl_2$ electrolyte with a melting point near 500°C enabled a Na-Zn metal battery to operate stably for 40 cycles. (Xu et al., 2016). In addition to these binary systems, multi-cationic systems have also been explored, often with the goal of reducing the solubility of Na in the electrolyte. A LiCl-NaCl-KCl molten salt electrolyte from Zhou *et al.* exhibited a melting point of ~400 °C and a Na^+ conductivity of 65 mS cm^{-1} at 450°C, and was used as the electrolyte in a Na|LiCl-NaCl-KCl|Bi_xSb cell cycled 700 times (Zhou et al., 2022). Phase diagrams and exchange reaction equilibria constants for the ternary system were also modeled by the same group (Ding et al., 2023). Another ternary system using iodide salts, LiI-NaI-KI, with a melting point of ~290 °C was demonstrated by Gong *et al.* and estimated to have a Na^+ conductivity of 28 mS cm^{-1} above 350°C (Gong et al., 2020). A low melting point (154°C) nitrate-based ternary molten salt, $NaNO_3$-KNO_3-$CsNO_3$, coupled with a BASE membrane enabled a molten Na-O_2 cell to operate at just 170°C for 400 cycles with no capacity fade (Zhu et al., 2022b). A similar triflate-based multi-cationic molten salt electrolyte has been demonstrated for high-temperature lithium batteries, and likely could find applications in molten Na batteries (Tu et al., 2010). Versatile molten salt chemistries using multiple components are a promising avenue for developing moderate-temperature electrolytes with tunable physical and electrochemical properties.

3.2.5 Alternative sodium ion conductors

In addition to the previous classes of electrolytes, a few emerging electrolytes could show promise for molten Na batteries. Na^+-conducting polymer electrolytes using Na salts in a polymer scaffold, such as polyethylene oxide (PEO), have been widely studied, but PEO often melts below 100°C and is susceptible to attack by molten Na. As such, polymer electrolytes have not yet been studied in molten Na batteries. As lower-temperature Na alloys are employed or advanced polymers are synthesized, there may be an opportunity for low-cost, mechanically tough, and easily processable electrolytes (Boschin and Johansson, 2015; Zhang et al., 2020b; Nimah et al., 2015; Koduru et al., 2016; Qiao et al., 2020). Polyborate salts emerged as a potential solid electrolyte when the high conductivity (100 mS cm^{-1} at 256°C) of $Na_2B_{12}H_{12}$ was reported by Udovic *et al.* in 2014. (Udovic et al., 2014). Since then, further studies of polyborates utilizing various anions (such as $NaCB_9H_{10}$, $NaCB_{11}H_{12}$, and $NaB_{11}H_{14}$ $Na(HCB_{11}H_5X_6)$ (X = Br or Cl), $Na_3B_{24}H_{23}$) have shed light on the high-temperature order-disorder transition and "paddle-wheel" conduction mechanism in these salts (Tang et al., 2016; Kweon et al., 2017; Tang et al., 2017; Jørgensen et al., 2020; Jin et al., 2023). These and other highly-

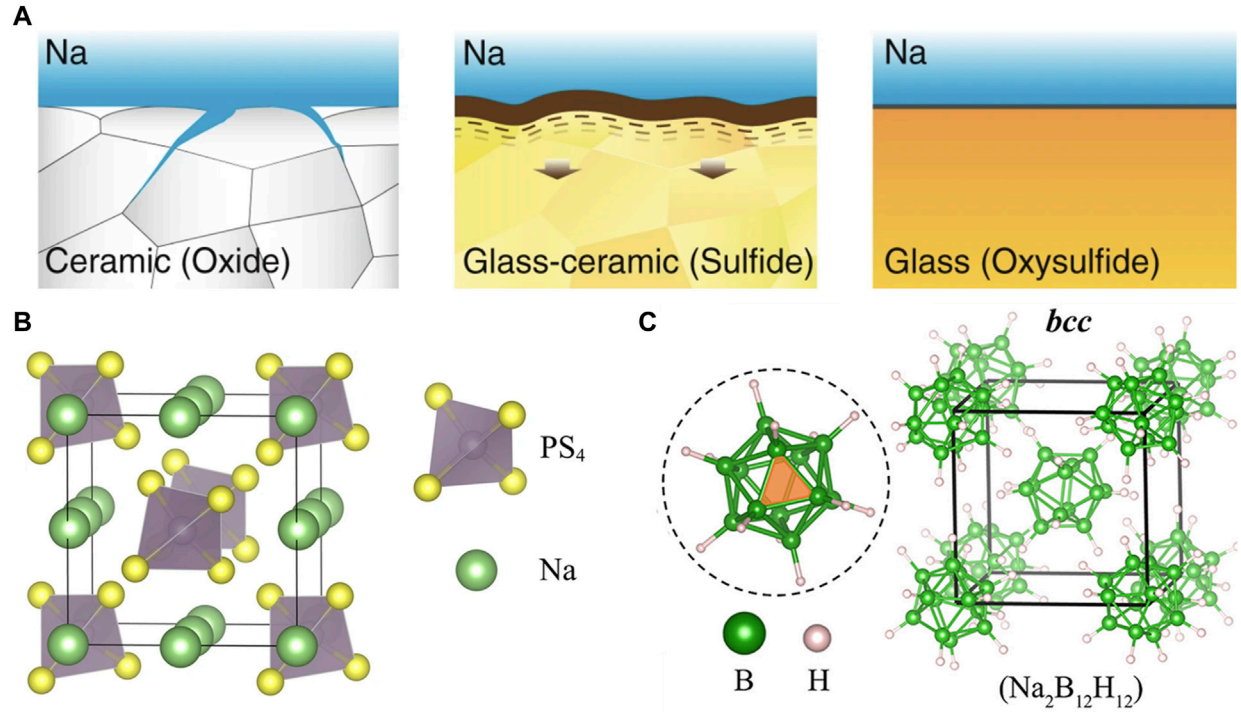

FIGURE 7
(A) Illustrations of ceramic, glass-ceramic, and glass microstructures and sodium interface behavior. Reprinted with permission from Ref. 201. **(B)** Structure of Na_3PS_4 electrolyte. Reprinted with permission from Ref. 225. **(C)** Structure of $Na_2B_{12}H_{12}$ electrolyte. Reprinted with permission from Ref. 238. Copyright 2017, American Chemical Society.

conductive salts may prove extremely valuable for molten Na batteries, particularly if their conductive phases can be stabilized at intermediate temperatures. Schematics and structures of these various sodium ion conductors are shown in Figure 7. A summary of electrolyte compositions, synthesis conditions, and resultant conductivities is provided in Table 3.

3.3 Na|Electrolyte interfaces

3.3.1 Mode I and II failure in solid electrolytes

In addition to the chemical reduction or amorphization that may occur in sodium solid electrolytes, applying potential and passing current may introduce further failure mechanisms in solid electrolytes. Electrochemical breakdown of BASE was first reported by Armstrong *et al.*, who observed sodium penetration (i.e., dendrites) through BASE in Na|BASE|Na symmetric cells above 100 mA cm^{-2} (Armstrong et al., 1974). The time to failure depended on both the current density (higher current → faster breakdown) and surface preparation (rougher surface → faster breakdown). The dependence on surface preparation suggested that surface flaws influenced dendrite formation. It was hypothesized that molten Na metal would preferentially wet and fill some surface pores and microcracks, depending on local geometry and surface chemistry. The features with good wetting (contact angle, $\theta < 90^{\circ}$) served as current concentrators, or "hotspots", where Na^+ ions were most likely to be deposited during electrolysis, leading to non-uniform current densities within the electrolyte. At these hotspots, the influx of Na metal could be greater than the diffusive transport that removed sodium from the region. If a hotspot was located at a pore or microcrack, the molten metal-filled feature could experience stress via Poiseuille pressure, which can be described by:

$$\Delta P = \frac{8\eta i V_m a^2}{nFb^3} \quad (14)$$

where ΔP is the Poiseuille pressure from the "flow" of metal (due to Na plating), η is the viscosity of molten Na metal, i is the applied current density, V_m is the molar volume of sodium, a is the crack length, n is the number of electrons in the reaction (1 for reduction of Na^+), F is the Faraday constant, and b is the crack tip radius (Armstrong et al., 1974) If this pressure reached a critical value, related to the fracture stress of electrolyte. This pressure-driven mechanism was termed Mode I failure (Figures 8A–C). Various authors have reported improvements to Eq. 14 to describe crack shapes more accurately and have extended its use to estimate the "critical" current density, at which Mode I failure will occur (Richman and Tennenhouse, 1975; Brennan, 1980; De Jonghe et al., 1981; Feldman and De Jonghe, 1982; Viswanathan and Virkar, 1982; Virkar and Viswanathan, 1983) In addition to the early reports of sharp cracks from surface imperfections, Mode I failure has also been observed as Na-filled cracks that are influenced by grain boundaries (Figure 8B) as well as large, diffusive fronts that extend from the stripping interface (Figure 8C).

Failure of Na solid electrolytes has also been observed at current densities considerably lower than those calculated to cause

TABLE 3 Summary of electrolyte compositions, synthesis conditions, and resultant conductivities. For the "Max Temp." columns, the maximum temperature during synthesis and the hold time necessary are listed. For conductivity, the lowest temperature that was reported in the original publication is listed here.

Year reference	Electrolyte	Max temp. (°C)	Time at max temp	Conductivity (°C)
2017 Lee et al. (2017)	BASE + YSZ	1,600	30 min	0.02 mS cm^{-1} (25)
2021 Dirksen et al. (2021)	BASE (TiO_2-doped)	1,500	30 min	300 mS cm^{-1} (300)
2015 Lu et al. (2015)	BASE + YSZ (TiO_2 & MnO_2-doped)	1,400	5 h	1.2 mS cm^{-1} (50)
2019 Li et al. (2019)	BASE + YSZ	1,530	10 min	160 mS cm^{-1} (300)
2014 Koganei et al. (2014)	BASE	1,400	15 min	19 mS cm^{-1} (25)
2020 Li et al. (2020b)	BASE	1,300	10 min	183 mS cm^{-1} (350)
2021 Li et al. (2021b)	BASE	1,100	10 min	70 mS cm^{-1} (350)
2021 Grady et al. (2021)	BASE (Mg-doped)	375	3 h	7.6 mS cm^{-1} (300)
2015 Jolley et al. (2015a)	NaSICON (Zn-doped)	1,150	12 h	0.81 mS cm^{-1} (25)
2017 Samiee et al. (2017)	NaSICON (Mg-doped)	1,230	24 h	2.7 mS cm^{-1} (25)
2020 Gross et al. (2020b)	NaSICON	1,230	12 h	2.0 mS cm^{-1} (25)
2021 Miao et al. (2021)	NaSICON (Y-doped)	1,100	6 h	1.2 mS cm^{-1} (25)
2019 Oh et al. (2019)	NaSICON	1,175	10 h	1.5 mS cm^{-1} (25)
2018 Noi et al. (2018)	NaSICON	900	10 h	1.0 mS cm^{-1} (25)
2018 Suzuki et al. (2018)	NaSICON	700	20 h	0.1 mS cm^{-1} (25)
2020 Grady et al. (2020)	NaSICON	386	3 h	0.25 mS cm^{-1} (25)
2018 Leng et al. (2018)	NaSICON (Mg-doped)	140	1 h	0.04 mS cm^{-1} (25)
2019 Leng et al. (2019)	NaSICON (Mg-doped)	850	6 h	0.11 mS cm^{-1} (25)
2023 Sozak et al. (2023)	NaSICON	1,200	5 h	1.5 x 10^{-3} mS cm^{-1} (25)
2016 Braga et al. (2016)	$Na_{2.99}Ba_{0.005}OCl_{1-x}(OH)_x$	250	3 h	10 mS cm^{-1} (25)
2022 Chi et al. (2022)	$Na_3PS_{4-x}O_x$	260	2 h	0.27 mS cm^{-1} (25)
2021 Keshri et al. (2021)	$Na_3Al_2P_{3-0.4x}Si_{0.5x}O_{12}$	1,620	2 h	3.3 x 10^{-4} mS cm^{-1} (100)
2022 Keshri et al. (2022)	$Na_3Al_{1.8}Si_{1.65}P_{1.8}O_{12}$	1,620	1 h	3.1 x 10^{-4} mS cm^{-1} (100)
2023 Olson et al. (2023)	$Na_4P_2S_{7-6x}O_{4.62x}N_{0.92x}$	780	6 h	5.0 x 10^{-3} mS cm^{-1} (25)
2014 Hayashi et al. (2014)	Na_3PS_4	270	2 h	0.46 mS cm^{-1} (25)
2014 Tanibata et al. (2014)	Na_3PS_4-Na_4SiS_4	220	2 h	0.74 mS cm^{-1} (25)
2018 Tanibata et al. (2018)	Na_3PS_4-Na_4GeS_4	330	2 h	0.02 mS cm^{-1} (25)
2018 Tsuji et al. (2018)	$Na_{10}GeP_2S_{12}$	450	1 h	0.01 mS cm^{-1} (25)
2019 Hayashi et al. (2019)	$Na_{2.88}Sb_{0.88}W_{0.12}S_4$	275	18 h	32 mS cm^{-1} (25)
2022 Zhou et al. (2022)	LiCl-NaCl-KCl (MS)	n/a	n/a	65 mS cm^{-1} (450)
2014 Udovic et al. (2014)	$Na_2B_{12}H_{12}$	350	4 h	100 mS cm^{-1} (256)
2023 Jin et al. (2023)	$Na_3B_{24}H_{23}$-$Na_2B_{12}H_{12}$	150	6 h	1.42 mS cm^{-1} (25)

BASE, β"-alumina solid electrolyte; YSZ, yttria-stabilized zirconia; MS = molten salt.

fracturing based on Eq. 14. De Jonghe *et al.* reported darkening in BASE used in Na-S cells during long duration testing (Jonghe et al., 1981). Reduction by Na metal increased BASE's electronic conductivity and allowed electrons to recombine with mobile Na^+ ions to form Na metal penetration during cycling. This electronic conductivity-driven failure has been termed Mode II failure (De Jonghe et al., 1981). In contrast to Mode I, Mode II failure points can occur near the plating interface (may be difficult to distinguish from Mode I), the stripping interface (Figure 8E), or anywhere within the interior of the electrolyte (Figure 8D). While Mode I was typically viewed as the predominant failure mechanism in molten Na cells, particularly at high current densities, recent works have emphasized the importance of Mode II. Hill *et al.* used unidirectional current tests to show that Mode I and Mode II sodium penetration occurred

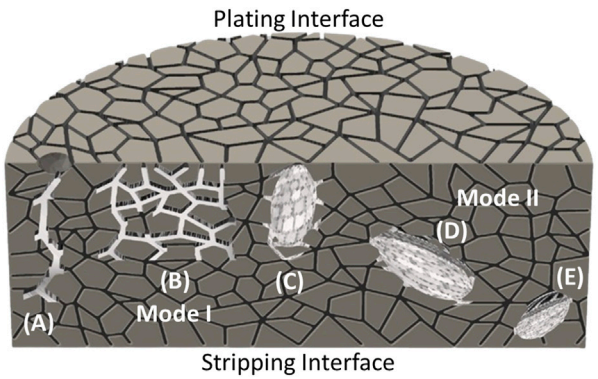

FIGURE 8
Illustration of Mode I and Mode II failure modes in solid electrolyte. Mode I has been observed as **(A)** large cracks stemming from surface imperfections, **(B)** grain boundaries filled with sodium, or **(C)** large, diffusive fronts that extend from the plating interface. Mode II has typically been observed as metal inclusions that stem from **(D)** the middle of the electrolyte interior or even **(E)** near the stripping interface.

significantly in NaSICON electrolytes at 100 mA cm^{-2}(110°C) (Hill et al., 2023). Subsequent *ex-situ* cross-sectional SEM imaging by the same group showed that Mode I could be mitigated at 500 mA cm^{-2} by using an interfacial coating, but Mode II was more difficult to suppress due to inherent electronic conductivity and microstructural features in NaSICON. The importance of Mode II has also been emphasized in electrolyte studies for solid-state batteries and its influence in molten Na batteries should be further explored (Han et al., 2019; Gorai et al., 2021; Wang et al., 2022; Shao et al., 2023). Detailed electrolyte studies utilizing unidirectional testing, conductivity vs. temperature series, and *operando* imaging would be beneficial to further understanding these important failure mechanisms (Fuchs et al., 2023; Counihan et al., 2024).

3.3.2 Interfacial coatings for solid electrolytes

One popular and effective strategy to mitigate solid electrolyte failure has been introducing interfacial coatings to facilitate uniform charge transfer between electrode and electrolyte. Better charge transfer could be due to enhanced wetting of liquid electrodes, improved interfacial contact for solid electrodes, or preventing the formation of less-conductive surface species at electrode-electrolyte interfaces (such as calcium-based impurities from BASE) (Lu et al., 2010b; Cheng et al., 2019; Cui et al., 2022; Gao et al., 2022). Particularly, a coating for the electrolyte|negative electrode (alkali metal) interface has been prioritized as it has been identified as the most susceptible to failure. Various authors have proposed coatings that typically relied on a porous carbon layer, a thin metal layer, or a combination of both (Hu et al., 2012; Ahlbrecht et al., 2017; Jin et al., 2019a; Gross et al., 2020b; Landmann et al., 2020). Generally, these coatings provide better wetting (smaller contact angle, θ) of Na metal and some level of electronic and ionic conductivity to assist interfacial charge transfer. These factors help to reduce localized current concentration and effective coatings have been found to increase the electrolyte's critical current density, resistance to Mode I failure, and overall cycle life (Hu et al., 2012; Ahlbrecht et al., 2017; Jin et al., 2019a; Gross et al., 2020b; Landmann et al., 2020).

Carbon-based coatings have been shown to significantly improve the performance of Na solid electrolytes and are commonly used in traditional ZEBRA batteries (Sudworth, 2001). Porous carbon can improve the contact angle between Na metal and the electrolyte and serve as a reservoir of Na metal during high-current operation. Hu *et al.* fabricated a porous carbon coating of ~6.6 μ m by reacting glucose and polymethyl methacrylate and casting onto BASE. The coating improved the wetting angle of molten Na from 151° to 95° at 300°C and enabled current densities up to 5.2 A cm^{-2} for 30 min intervals in Na symmetric cells. Thicker coatings of carbon black and sodium hexametaphosphate (50–200 μ m) deposited via spray coating by Landmann *et al.* also improved wetting and allowed current densities up to 2.6 A cm^{-2} and a cumulative capacity of >10 Ah cm^{-2} before failure. Other carbon-based coatings, such as sparked reduced graphene oxide and carbon paste have been shown to improve cycling and high current performance in sodium batteries that use BASE. (Kim et al., 2015c; Jin et al., 2019b). To the best of our knowledge, no reports of purely carbon-based coatings have been published for molten sodium batteries using NaSICON, but a report of a fluorinated amorphous carbon layer on NaSICON for room-temperature sodium batteries may provide insight to designing such a coating. (Zhang et al., 2021). Purely carbon-based coatings typically represent the least expensive coating option and, with further improvement (particularly for NaSICON), would be a desirable option for low-cost, high-performance molten Na batteries.

Metal and metal oxide coatings are another potentially effective approach to improving solid electrolyte performance. Recent reports from Hu *et al.* highlighted Ni nanowires (2013) and iron oxide (2014) as excellent coatings, enabling current densities up to 1.5 and 3.9 A cm^{-2}, respectively. The group proposed that the high current densities resulted from higher surface energy metals providing better inherent wetting and more surface area for wetting (Hu et al., 2013; Hu et al., 2014). However, this review was not able to identify any further works utilizing Ni- or Fe-based coatings for molten Na batteries. The lack of further Ni- and Fe-based coating reports seems to be, at least partially, due to the recognition of chemical reactivity as an influential factor in coating performance. Metals that are known to react with Na, such as Pb, Sn, Bi, and In, have been identified as potential interfacial coatings. In 2013, Reed *et al.* showed that sputtered Sn coatings enabled complete molten Na wetting ($\theta \rightarrow 0$) on BASE at 200°C (Reed et al., 2013). Eventually, Gross *et al.* reported that a sputtered Sn coating could also improve molten Na wetting and current density capability using NaSICON electrolytes, even at the low temperature of 110°C. It was shown that the molten Na and Sn coating formed a NaSn intermetallic phase upon conditioning at low current densities. This NaSn phase was proposed to effectively wet Na metal and provide ample ionic and electronic conductivity to enable high current densities up to 50 mA cm^{-2} (Gross et al., 2020b). Higher-current testing of the Sn coating showed that Mode I failure could be mitigated at current densities as high as 500 mA cm^{-2} (Hill et al., 2024). Pb-based coatings deposited on BASE from the decomposition of lead acetate trihydrate have similarly shown improved wetting and

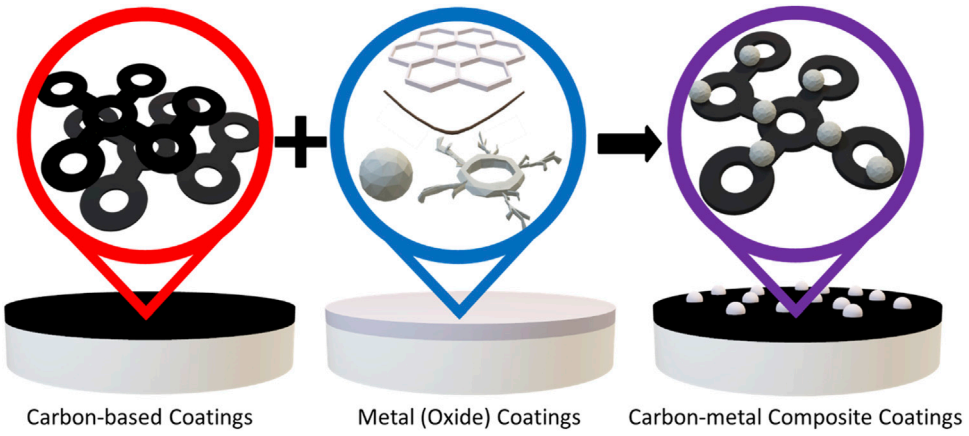

FIGURE 9
Illustration of general coating approaches used for molten Na|solid electrolyte interfaces. Various studies have reported using carbon-based coatings, metal (oxide) coatings, and composite carbon-metal coatings.

current densities above 175°C. The formation of Na-Pb alloys observed by Chang *et al.* upon contact between Na and Pb metal was suggested to contribute significantly to the improved performance. The same study performed an in-depth analysis of the wetting behavior of molten Na and emphasized the importance of the "sunny-side-up"-shaped sodium wetting, suggesting that a thin film of Na likely forms quickly within the film, initiating the desired wetting behavior (Chang et al., 2018b). Studies exploring Bi and In-based coatings from Ahlbrecht *et al.* yielded positive wetting results from Bi coatings but no positive wetting effect from In coatings at temperatures below 125°C, suggesting that chemical reactivity is not the sole requirement for an effective coating material (Ahlbrecht et al., 2017). Bi-islands coatings fabricated by Jin *et al.* also successfully improved wetting and cycling performance in Na-$NiCl_2$ cells, highlighting the effectiveness Bi-based metal coatings (Jin et al., 2019a). Recently, Sn-, Pb-, and Bi-based metal coatings have been the most widely reported coatings, with each metal having its own potential advantages in terms of cost, toxicity, and sodium wettability.

Based on the success of carbon and metal-based coatings, it is logical that a composite carbon-metal coating could provide better overall performance based on benefits from each of the components. Composite coatings of Pb or Sn nanoparticles in a porous carbon black matrix were fabricated by Li *et al.* and both coatings showed fast sodium wetting and wicking at 120°C. The enhanced wetting at lower temperatures was attributed to the higher surface area contributed by the carbon black along with the alloying behavior of the Pb or Sn particles. (Li et al., 2022). Weller *et al.* later applied the same coating to BASE and NaSICON for use in Na-Al batteries. (Weller et al., 2023). Further studies into molten sodium behavior with composite carbon-metal coatings were not found in this review, but another three-dimensional cross-linking carbon fiber decorated with Sn nanoparticles has been used to improve current density in RT β"-alumina batteries and could provide insight to further improvements in molten sodium batteries (Lai et al., 2022). Using inexpensive carbon matrices as hosts for alloying metal particles also has the potential to lower the total amount of metal in the coating compared to pure metal-based coatings to significantly lower costs. The lower-cost and synergistic behavior of the carbon-metal composite coatings make them an interesting future direction.

The general coating approaches applied by researchers are illustrated in Figure 9. A summary of coated electrolyte systems and the maximum current density reported with them is also provided in Table 4. It is important to note that many of these studies did not explicitly search for a maximum current density and the coatings in these studies provide other potential benefits, such as improved wettability and cycle life, as discussed in the text.

4 Summary and outlook

Molten Na batteries are promising stationary and grid-scale energy storage technologies with a long history of development and a recent acceleration of renewed innovation. The natural abundance of many of the elements used in molten Na batteries make them particularly attractive for grid-scale, long-duration energy storage and will help to realize a clean, reliable, and resilient electrical grid. Various technologies, including Na-S and ZEBRA-style batteries, are already contributing to stationary storage solutions and many more technologies are on the horizon. Lower temperature chemistries have the potential to operate below 120°C and further reduce costs for grid-scale storage. Na-alloy negative electrodes could push operating temperatures even closer to room temperature. Emerging molten Na flow batteries can design unique cell stacks that decouple energy and power density to meet the diverse demands of the electrical grid. To enable these new batteries, many advancements have been made in solid electrolyte chemistries, manufacturing, and interface regulation. Lower-temperature sintering and thin electrolyte fabrication l ower costs, while aliovalent doping and interfacial coatings create high-conductivity, dendrite-resistant electrolytes. As researchers continue to make breakthroughs in electrodes, electrolytes, and, critically, the interfaces between them, molten Na batteries will become a staple of the electrical grid of the future.

TABLE 4 Summary of interfacial coatings and their maximum current density at the given temperature in recent molten Na battery reports.

Year reference	Electrolyte material	Coating material	Temp. (°C)	Current density (mA cm^{-2})
2012 Hu et al. (2012)	BASE	Porous Carbon	350	5,200
2013 Hu et al. (2013)	BASE	Nickel Nanowire Network	350	1,500
2014 Hu et al. (2014)	BASE	Porous Iron Oxide	350	3,900
2014 Lu et al. (2014)	BASE	Lead Oxide	150–175	10
2017 Ahlbrecht et al. (2017)	BASE	Tin, Bismuth, and Indium Metal	105–150	10
2018 Chang et al. (2018b)	BASE	Lead Metal Microspheres	190	10
2018 Jung et al. (2018)	BASE	Lead Metal Microspheres	190	50
2019 Jin et al. (2019b)	BASE	Reduced Graphene Oxide	175	20
2019 Jin et al. (2019a)	BASE	Bismuth Metal Islands	175	1.7
2020 Landmann et al. (2020)	BASE	Porous Carbon + Sodium Hexametaphosphate	250	2,600
2020 Gross et al. (2020b)	NaSICON	Tin Metal	110	50
2022 Li et al. (2022)	BASE	Porous Carbon + Lead/Tin (Oxide) Nanoparticles	110–150	15
2023 Weller et al. (2023)	BASE/NaSICON	Porous Carbon + Lead (Oxide) Nanoparticles	180	20
2023 Maraschky et al. (2023a)	NaSICON	Tin Metal	110	2.5
2024 Hill et al. (2024)	NaSICON	Tin Metal	110	500

BASE, β”-alumina solid electrolyte.

Author contributions

RH: Visualization, Writing–original draft, Writing–review and editing. MG: Visualization, Writing–review and editing. SP: Writing–review and editing. AP: Writing–review and editing. LS: Writing–review and editing. ES: Writing–review and editing. Y-TC: Writing–review and editing.

Funding

The author(s) declare that no financial support was received for the research, authorship, and/or publication of this article.

Acknowledgments

The authors would like to acknowledge the support of the Energy Storage Program, managed by Der. Imre Gyuk, in the U.S. Department of Energy's Office of Electricity. Sandia National Laboratories is a multi-mission laboratory managed and operated by National Technology & Engineering Solutions of Sandia, LLC (NTESS), a wholly owned subsidiary of Honeywell International Inc., for the U.S. Department of Energy's National Nuclear Security Administration (DOE/NNSA) under contract DE-NA0003525. This written work is authored by an employee of NTESS. The employee, not NTESS, owns the right, title and interest in and to the written work and is responsible for its contents. The publisher acknowledges that the U.S. Government retains a non-exclusive, paid-up, irrevocable, world-wide license to publish or reproduce the published form of this written work or allow others to do so, for U.S. Government purposes. The DOE will provide public access to results of federally sponsored research in accordance with the DOE Public Access Plan.

Conflict of interest

The authors declare that the research was conducted in the absence of any commercial or financial relationships that could be construed as a potential conflict of interest.

The author(s) declared that they were an editorial board member of Frontiers, at the time of submission. This had no impact on the peer review process and the final decision.

Publisher's note

Author disclaimer

Any subjective views or opinions that might be expressed in the written work do not necessarily represent the views of the U.S. Government.

References

Ackermann, T., and Söder, L. (2000). Wind energy technology and current status: a review. *Renew. Sustain. Energy Rev.* 4 (4), 315–374. doi:10.1016/S1364-0321(00)00004-6

Ahlbrecht, K., Bucharsky, C., Holzapfel, M., Tübke, J., and Hoffmann, M. J. (2017). Investigation of the wetting behavior of Na and Na alloys on uncoated and coated Na-β-alumina at temperatures below 150 °C. *Ionics* 23 (5), 1319–1327. doi:10.1007/s11581-017-2017-x

Ahn, B.-M., Ahn, C.-W., Hahn, B.-D., Choi, J.-J., Kim, Y.-D., Lim, S.-K., et al. (2019). Easy approach to realize low cost and high cell capacity in sodium nickel-iron chloride battery. *Compos. Part B Eng.* 168, 442–447. doi:10.1016/j.compositesb.2019.03.064

Albertus, P., Manser, J. S., and Litzelman, S. (2020). Long-duration electricity storage applications, economics, and technologies. *Joule* 4 (1), 21–32. doi:10.1016/j.joule.2019.11.009

Allu, A. R., Balaji, S., and Annapurna, K. (2018). Electrical and mechanical properties of $Na_{2.8}Ca_{0.1}Al_2Ga_{0.5}P_{2.7}O_{12}$ glass based electrolyte materials: influence of Ag+ ion-exchange. *J. Non-Crystalline Solids* 498, 323–330. doi:10.1016/j.jnoncrysol.2018.03.043

Almond, D. P., West, A. R., and Grant, R. J. (1982). Temperature dependence of the a.c. conductivity of Naβ-alumina. *Solid State Commun.* 44, 1277–1280. doi:10.1016/0038-1098(82)91103-6

Andres, R. J., Boden, T. A., Bréon, F. M., Ciais, P., Davis, S., Erickson, D., et al. (2012). A synthesis of carbon dioxide emissions from fossil-fuel combustion. *Biogeosciences* 9 (5), 1845–1871. doi:10.5194/bg-9-1845-2012

Anvari, M., Lohmann, G., Wächter, M., Milan, P., Lorenz, E., Heinemann, D., et al. (2016). Short term fluctuations of wind and solar power systems. *New J. Phys.* 18 (6), 063027. doi:10.1088/1367-2630/18/6/063027

Ao, X., Wen, Z., Hu, Y., Wu, T., Wu, X., and He, Q. (2017a). Enhanced cycle performance of a Na/$NiCl_2$ battery based on Ni particles encapsulated with Ni_3S_2 layer. *J. Power Sources* 340, 411–418. doi:10.1016/j.jpowsour.2016.11.091

Ao, X., Wen, Z., Wu, X., Wu, T., and Wu, M. (2017b). Self-repairing function of Ni_3S_2 layer on Ni particles in the Na/$NiCl_2$ cells with the addition of sulfur in the catholyte. *ACS Appl. Mat. Interfaces* 9 (25), 21234–21242. doi:10.1021/acsami.7b03873

Archer, D., Eby, M., Brovkin, V., Ridgwell, A., Cao, L., Mikolajewicz, U., et al. (2009). Atmospheric lifetime of fossil fuel carbon dioxide. *Annu. Rev. Earth Planet. Sci.* 37 (1), 117–134. doi:10.1146/annurev.earth.031208.100206

Armstrong, R. D., Dickinson, T., and Turner, J. (1974). The breakdown of β-alumina ceramic electrolyte. *Electrochimica Acta* 19 (5), 187–192. doi:10.1016/0013-4686(74)85065-6

Arnold, B. J. (2023). "1 - coal formation," in *The coal handbook* Editor D Osborne. Second Edition (Sawston, United Kingdom: Woodhead Publishing), 3–21.

Balat, M. A. (2009). A review of modern wind turbine technology. *Energy Sources, Part A Recovery, Util. Environ. Eff.* 31 (17), 1561–1572. doi:10.1080/15567030802094045

Barison, S., Fasolin, S., Mortalò, C., Boldrini, S., and Fabrizio, M. (2015). Effect of precursors on β-alumina electrolyte preparation. *J. Eur. Ceram. Soc.* 35 (7), 2099–2107. doi:10.1016/j.jeurceramsoc.2015.01.006

Bates, J. B., Engstrom, H., Wang, J. C., Larson, B. C., Dudney, N. J., and Brundage, W. E. (1981). Composition, ion-ion correlations and conductivity of beta″-alumina. *Solid State Ionics* 5, 159–162. doi:10.1016/0167-2738(81)90217-4

Bay, M.-C., Wang, M., Grissa, R., Heinz, M. V. F., Sakamoto, J., and Battaglia, C. (2020). Sodium plating from Na-β″-Alumina ceramics at room temperature, paving the way for fast-charging all-solid-state batteries. *Adv. Energy Mater.* 10 (3), 1902899. doi:10.1002/aenm.201902899

Beevers, C., and Ross, M. A. S. (1937). The crystal structure of "beta alumina" $Na_2O{\cdot}11Al_2O_3$. *Z. für Kristallogr. Mater.* 97 (1-6), 59–66. doi:10.1524/zkri.1937.97.1.59

Bell, N. S., Edney, C., Wheeler, J. S., Ingersoll, D., and Spoerke, E. D. (2014). The influences of excess sodium on low-temperature NaSICON synthesis. *J. Am. Ceram. Soc.* 97 (12), 3744–3748. doi:10.1111/jace.13167

Bernard, A. (1960). *Regenerative battery*. United States: United States US3245836A.

Bhandari, R., Kumar, B., and Mayer, F. (2020). Life cycle greenhouse gas emission from wind farms in reference to turbine sizes and capacity factors. *J. Clean. Prod.* 277, 123385. doi:10.1016/j.jclepro.2020.123385

Bloom, I., Kucera, G., Bradley, J., Nelson, P., and Roche, M. (1986). *Low-resistivity glass electrolytes for sodium-sulfur cells*. USA: Argonne National Lab., IL.

Bock, J. A., Spoerke, E. D., Brown-Shaklee, H. J., and Small, L. J. (2023). Solution-assisted densification of NaSICON ceramics. *U. S. U.S. Pat. no. 11/600* 856.

Boilot, J. P., Collin, G., and Colomban, P. (1987). Crystal structure of the true nasicon: $Na_3Zr_2Si_2PO_{12}$. *Mater. Res. Bull.* 22 (5), 669–676. doi:10.1016/0025-5408(87)90116-4

Boilot, J. P., Collin, G., and Colomban, P. (1988). Relation structure-fast ion conduction in the NASICON solid solution. *J. Solid State Chem.* 73 (1), 160–171. doi:10.1016/0022-4596(88)90065-5

Bones, R. J., Teagle, D. A., Brooker, S. D., and Cullen, F. L. (1989). Development of a Ni, $NiCl_2$ positive electrode for a liquid sodium (ZEBRA) battery cell. *J. Electrochem. Soc.* 136 (5), 1274–1277. doi:10.1149/1.2096905

Boschin, A., and Johansson, P. (2015). Characterization of NaX (X: TFSI, FSI)–PEO based solid polymer electrolytes for sodium batteries. *Electrochimica Acta* 175, 124–133. doi:10.1016/j.electacta.2015.03.228

Braga, M. H., Murchison, A. J., Ferreira, J. A., Singh, P., and Goodenough, J. B. (2016). Glass-amorphous alkali-ion solid electrolytes and their performance in symmetrical cells. *Energy & Environ. Sci.* 9 (3), 948–954. doi:10.1039/c5ee02924d

Brennan, M. P. J. (1980). The failure of beta-alumina electrolyte by a dendritic penetration mechanism. *Electrochimica Acta* 25, 621–627. doi:10.1016/0013-4686(80)87067-8

Burnham, A. K., and Braun, R. L. (1990). Development of a detailed model of petroleum formation, destruction, and expulsion from lacustrine and marine source rocks. *Org. Geochem.* 16 (1), 27–39. doi:10.1016/0146-6380(90)90023-S

Calero, I., Cañizares, C. A., Bhattacharya, K., and Baldick, R. (2022). Duck-curve mitigation in power grids with high penetration of PV generation. *IEEE Trans. Smart Grid* 13 (1), 314–329. doi:10.1109/TSG.2021.3122398

Certo, J., Furtado, C. S., Ferreira, A. J., and Perdigão, J. M. (1998). Na-β Alumina powder processing by a Na_2CO_3 precipitation method. *Ionics* 4 (1-2), 124–128. doi:10.1007/bf02375790

Chang, H.-J., Canfield, N. L., Jung, K., Sprenkle, V. L., and Li, G. (2017). Advanced Na-$NiCl_2$ battery using nickel-coated graphite with core–shell microarchitecture. *ACS Appl. Mat. Interfaces* 9 (13), 11609–11614. doi:10.1021/acsami.7b00271

Chang, H. J., Lu, X., Bonnett, J. F., Canfield, N. L., Han, K., Engelhard, M. H., et al. (2018b). Decorating β″-alumina solid-state electrolytes with micron Pb spherical particles for improving Na wettability at lower temperatures. *J. Mat. Chem. A* 6, 19703–19711. doi:10.1039/C8TA06745G

Chang, H. J., Lu, X., Bonnett, J. F., Canfield, N. L., Son, S., Park, Y. C., et al. (2018a). Ni-less cathodes for high energy density, intermediate temperature Na–$NiCl_2$ batteries. *Adv. Mater. Interfaces* 5 (10), 1701592. doi:10.1002/admi.201701592

Chen, Y., Kang, Y., Zhao, Y., Wang, L., Liu, J., Li, Y., et al. (2021). A review of lithium-ion battery safety concerns: the issues, strategies, and testing standards. *J. Energy Chem.* 59, 83–99. doi:10.1016/j.jechem.2020.10.017

Cheng, Q., Li, A., Li, N., Li, S., Zangiabadi, A., Li, T. D., et al. (2019). Stabilizing solid electrolyte-anode interface in Li-metal batteries by boron nitride-based nanocomposite coating. *Joule* 3 (6), 1510–1522. doi:10.1016/j.joule.2019.03.022

Chi, C., Katsui, H., and Goto, T. (2017). Effect of Li addition on the formation of Na-β/β″-alumina film by laser chemical vapor deposition. *Ceram. Int.* 43 (1), 1278–1283. Part B). doi:10.1016/j.ceramint.2016.10.077

Chi, X., Zhang, Y., Hao, F., Kmiec, S., Dong, H., Xu, R., et al. (2022). An electrochemically stable homogeneous glassy electrolyte formed at room temperature for all-solid-state sodium batteries. *Nat. Commun.* 13 (1), 2854. doi:10.1038/s41467-022-30517-y

Choy, J.-H., Yoo, J.-S., Han, Y.-S., and Kim, Y.-H. (1993). Citrate sol-gel method for the preparation of β/β′-alumina. *Mater. Lett.* 16 (4), 226–230. doi:10.1016/0167-577X(93)90169-X

Chu, I.-H., Kompella, C. S., Nguyen, H., Zhu, Z., Hy, S., Deng, Z., et al. (2016). Room-temperature all-solid-state rechargeable sodium-ion batteries with a Cl-doped Na_3PS_4 superionic conductor. *Sci. Rep.* 6 (1), 33733. doi:10.1038/srep33733

Coetzer, J. (1986). A new high energy density battery system. *J. Power Sources* 18 (4), 377–380. doi:10.1016/0378-7753(86)80093-3

Counihan, M. J., Chavan, K. S., Barai, P., Powers, D. J., Zhang, Y., Srinivasan, V., et al. (2024). The phantom menace of dynamic soft-shorts in solid-state battery research. *Joule* 8, 64–90. doi:10.1016/j.joule.2023.11.007

Cross, A. T., and Phillips, T. L. (1990). Coal-forming through time in north America. *Int. J. Coal Geol.* 16 (1), 1–46. doi:10.1016/0166-5162(90)90012-N

Crouthamel, C. E., and Recht, H. L. (1967). *Regenerative EMF cells*. Washington, D.C.: ACS Publications.

Cui, C., Zeng, C., Huang, G., Feng, X., Zhang, Y., Zhai, T., et al. (2022). *In situ* visualizing the interfacial failure mechanism and modification promotion of LAGP solid electrolyte toward Li metal anode. *Adv. Energy Mater.* 12 (41), 2202250. doi:10.1002/aenm.202202250

De Jonghe, L. C., Feldman, L., and Buechele, A. (1981). Failure modes of Na-beta alumina. *Solid State Ionics* 5, 267–269. doi:10.1016/0167-2738(81)90244-7

Dell, R., and Moseley, P. (1981). Beta-alumina electrolyte for use in sodium/sulphur batteries: Part I. Fundamental properties. *J. Power Sources* 6 (2), 143–160. doi:10.1016/0378-7753(81)80020-1

Denholm, P., Cole, W., and Blair, N. (2023). *Moving beyond 4-hour Li-ion batteries: challenges and opportunities for long (er)-Duration energy storage*. United States: NREL is a national laboratory of the U.S. Department of Energy.

Denholm, P., Nunemaker, J., Gagnon, P., and Cole, W. (2020). The potential for battery energy storage to provide peaking capacity in the United States. *Renew. Energy* 151, 1269–1277. doi:10.1016/j.renene.2019.11.117

Ding, W., Gong, Q., Liang, S., Hoffmann, R., Zhou, H., Li, H., et al. (2023). Multi-cationic molten salt electrolyte of high-performance sodium liquid metal battery for grid storage. *J. Power Sources* 553, 232254. doi:10.1016/j.jpowsour.2022.232254

Ding, Y., Guo, X., Qian, Y., Xue, L., Dolocan, A., and Yu, G. (2020a). Room-temperature all-liquid-metal batteries based on fusible alloys with regulated interfacial chemistry and wetting. *Adv. Mater.* 32 (30), 2002577. doi:10.1002/adma.202002577

Ding, Y., Guo, X., Qian, Y., and Yu, G. (2020b). Low-temperature multielement fusible alloy-based molten sodium batteries for grid-scale energy storage. *ACS Cent. Sci.* 6 (12), 2287–2293. doi:10.1021/acscentsci.0c01035

Dirksen, C. L., Skadell, K., Schulz, M., Fertig, M. P., and Stelter, M. (2021). Influence of 3d transition metal doping on lithium stabilized Na-β″-Alumina solid electrolytes. *Materials* 14 (18), 5389. doi:10.3390/ma14185389

Dustmann, C.-H. (2004). Advances in ZEBRA batteries. *J. Power Sources* 127 (1), 85–92. doi:10.1016/j.jpowsour.2003.09.039

Ediger, V. Ş. (2019). An integrated review and analysis of multi-energy transition from fossil fuels to renewables. *Energy Procedia* 156, 2–6. doi:10.1016/j.egypro.2018.11.073

El Chaar, L., lamont, L. A., and El Zein, N. (2011). Review of photovoltaic technologies. *Renew. Sustain. Energy Rev.* 15 (5), 2165–2175. doi:10.1016/j.rser.2011.01.004

Engstrom, H., Bates, J., Brundage, W., and Wang, J. (1981). Ionic conductivity of sodium beta ″-alumina. *Solid State Ionics* 2 (4), 265–276. doi:10.1016/0167-2738(81)90027-8

Enlighten (2023). Enlighten. https://enlighteninc.com/ (Accessed December 30, 2023).

Feldman, L. A., and De Jonghe, L. C. (1982). Initiation of mode I degradation in sodium-beta alumina electrolytes. *J. Mat. Sci.* 17, 517–524. doi:10.1007/BF00591486

Fertig, M. P., Skadell, K., Schulz, M., Dirksen, C., Adelhelm, P., and Stelter, M. (2022). From high-to low-temperature: the revival of sodium-beta alumina for sodium solid-state batteries. *Batter. Supercaps* 5, e202100131. doi:10.1002/BATT.202100131

Fertig, M. P., Skadell, K., Wegner, K., Schulz, M., and Stelter, M. (2023). A medium-temperature all-solid-state sodium battery utilizing sodium-beta alumina and a polymeric composite positive electrode. *J. Electrochem. Soc.* 170 (5), 050501. doi:10.1149/1945-7111/accf39

Flynn, A., Taggert, D., Johnston, J., Christensen, M., Makowski, M., Moss, R., et al. (2022). "Novel sodium – polysulfide flow battery grid-scale energy storage technology," in 2022 IEEE Electrical Energy Storage Application and Technologies Conference, Austin, Texas, USA, 8-9 Nov. 2022, 1–3. doi:10.1109/EESAT55007.2022.9998026

Frusteri, L., Leonardi, S. G., Samperi, M., Antonucci, V., and D'Urso, C. (2022). Characterization and testing of cathode materials for high temperature sodium nickel-iron chloride battery. *J. Energy Storage* 55, 105503. doi:10.1016/j.est.2022.105503

Fuchs, T., Culver, S. P., Till, P., and Zeier, W. G. (2020). Defect-mediated conductivity enhancements in $Na_{3-x}Pn_{1-x}W_xS_4$ (pn = P, Sb) using aliovalent substitutions. *ACS Energy Lett.* 5 (1), 146–151. doi:10.1021/acsenergylett.9b02537

Fuchs, T., Haslam, C. G., Richter, F. H., Sakamoto, J., and Janek, J. (2023). Evaluating the use of critical current density tests of symmetric lithium transference cells with solid electrolytes. *Adv. Energy Mater.* 13 (45), 2302383. doi:10.1002/aenm.202302383

Fuentes, R. O., Figueiredo, F. M., Marques, F. M. B., and Franco, J. I. (2001). Influence of microstructure on the electrical properties of NASICON materials. *Solid State Ionics* 140 (1), 173–179. doi:10.1016/S0167-2738(01)00701-9

Fzsonick (2023a). *Green & safe salt battery*. https://www.fzsonick.com/home (Accessed December 30, 2023).

Fzsonick (2023b). *Industrial energy storage*. https://www.fzsonick.com/applications/industrial-energy-storage (Accessed December 30, 2023).

Gandi, S., Chinta, S. R., Ojha, P. K., Surendra Babu, M. S., and Ravuri, B. R. (2018). High Na-ion conducting $Na_{1+x}[Sn_xGe_{2-x}(PO_4)_3]$ glass-ceramic electrolytes: structural and electrochemical impedance studies. *J. Am. Ceram. Soc.* 101 (1), 167–177. doi:10.1111/jace.15103

Gao, L., Chen, J., Chen, Q., and Kong, X. (2022). The chemical evolution of solid electrolyte interface in sodium metal batteries. *Sci. Adv.* 8 (6), eabm4606. doi:10.1126/sciadv.abm4606

Gao, X., Hu, Y., Li, Y., Wang, J., Wu, X., Yang, J., et al. (2020). High-rate and long-life intermediate-temperature Na–NiCl2 battery with dual-functional Ni–carbon composite nanofiber network. *ACS Appl. Mat. Interfaces* 12 (22), 24767–24776. doi:10.1021/acsami.0c04470

Gardner, P., Jones, F., Rowe, M., Nouri, A., and van de Vegte, H. (2016). *E-storage: shifting from cost to value Wind and solar applications*. London, United Kingdom: World Energy Council.

Gerbig, F., Holzapfel, M., and Nirschl, H. (2023). Simulating the impact of glassy carbon foam electrodes on the performance of sodium iodine batteries. *J. Electrochem. Soc.* 170 (4), 040517. doi:10.1149/1945-7111/accab7

Gerovasili, E., May, J. F., and Sauer, D. U. (2014). Experimental evaluation of the performance of the sodium metal chloride battery below usual operating temperatures. *J. Power Sources* 251, 137–144. doi:10.1016/j.jpowsour.2013.11.046

Gong, Q., Ding, W., Bonk, A., Li, H., Wang, K., Jianu, A., et al. (2020). Molten iodide salt electrolyte for low-temperature low-cost sodium-based liquid metal battery. *J. Power Sources* 475, 228674. doi:10.1016/j.jpowsour.2020.228674

Gong, Z., Shu, L., Yin, J., Gao, C., Liu, Y., Zhou, X., et al. (2023). Double-substituted Na_3SbS_4 Glass–Ceramic electrolyte with excellent performance for sodium-ion batteries. *Ceram. Int.* 49 (23), 37445–37453. doi:10.1016/j.ceramint.2023.09.070

Goodenough, J. B., Hong, H. Y. P., and Kafalas, J. A. (1976). Fast Na+-ion transport in skeleton structures. *Mater. Res. Bull.* 11, 203–220. doi:10.1016/0025-5408(76)90077-5

Gorai, P., Famprikis, T., Singh, B., Stevanović, V., and Canepa, P. (2021). Devil is in the defects: electronic conductivity in solid electrolytes. *Chem. Mat.* 33 (18), 7484–7498. doi:10.1021/acs.chemmater.1c02345

Grady, Z., Ndayishimiye, A., and Randall, C. (2021). A dramatic reduction in the sintering temperature of the refractory sodium β″-alumina solid electrolyte via cold sintering. *J. Mat. Chem. A* 9 (38), 22002–22014. doi:10.1039/d1ta05933e

Grady, Z. M., Tsuji, K., Ndayishimiye, A., Hwan-Seo, J., and Randall, C. A. (2020). Densification of a solid-state NASICON sodium-ion electrolyte below 400 °C by cold sintering with a fused hydroxide solvent. *ACS Appl. Energy Mater.* 3 (5), 4356–4366. doi:10.1021/acsaem.0c00047

Gross, M. M., and Manthiram, A. (2019). Development of low-cost sodium-aqueous polysulfide hybrid batteries. *Energy Storage Mater.* 19, 346–351. doi:10.1016/j.ensm.2019.03.026

Gross, M. M., Percival, S. J., Lee, R. Y., Peretti, A. S., Spoerke, E. D., and Small, L. J. (2021). A high-voltage, low-temperature molten sodium battery enabled by metal halide catholyte chemistry. *Cell Rep. Phys. Sci.* 2 (7), 100489. ARTN 100489. doi:10.1016/j.xcrp.2021.100489

Gross, M. M., Percival, S. J., Small, L. J., Lamb, J., Peretti, A. S., and Spoerke, E. D. (2020a). Low-temperature molten sodium batteries. *ACS Appl. Energy Mater.* 3 (11), 11456–11462. doi:10.1021/acsaem.0c02385

Gross, M. M., Small, L. J., Peretti, A. S., Percival, S. J., Rodriguez, M. A., and Spoerke, E. D. (2020b). Tin-based ionic chaperone phases to improve low temperature molten sodium-NaSICON interfaces. *J. Mat. Chem. A* 8, 17012–17018. doi:10.1039/d0ta03571h

Guerra, O. J. (2021). Beyond short-duration energy storage. *Nat. Energy* 6 (5), 460–461. doi:10.1038/s41560-021-00837-2

Guin, M., and Tietz, F. (2015). Survey of the transport properties of sodium superionic conductor materials for use in sodium batteries. *J. Power Sources* 273, 1056–1064. doi:10.1016/j.jpowsour.2014.09.137

Han, F., Westover, A. S., Yue, J., Fan, X., Wang, F., Chi, M., et al. (2019). High electronic conductivity as the origin of lithium dendrite formation within solid electrolytes. *Nat. Energy* 4, 187–196. doi:10.1038/s41560-018-0312-z

Hayashi, A., Masuzawa, N., Yubuchi, S., Tsuji, F., Hotehama, C., Sakuda, A., et al. (2019). A sodium-ion sulfide solid electrolyte with unprecedented conductivity at room temperature. *Nat. Commun.* 10 (1), 5266. doi:10.1038/s41467-019-13178-2

Hayashi, A., Noi, K., Sakuda, A., and Tatsumisago, M. (2012). Superionic glass-ceramic electrolytes for room-temperature rechargeable sodium batteries. *Nat. Commun.* 3 (1), 856. doi:10.1038/ncomms1843

Hayashi, A., Noi, K., Tanibata, N., Nagao, M., and Tatsumisago, M. (2014). High sodium ion conductivity of glass–ceramic electrolytes with cubic Na3PS4. *J. Power Sources* 258, 420–423. doi:10.1016/j.jpowsour.2014.02.054

Heinz, M. V. F., Sieuw, L., Lan, T., Turconi, A., Basso, D., Vagliani, F., et al. (2023). Cell design strategies for sodium-zinc chloride (Na-$ZnCl_2$) batteries, and first demonstration of tubular cells with 38 Ah capacity. *Electrochimica Acta* 464, 142881. doi:10.1016/j.electacta.2023.142881

Helbig, C., Bradshaw, A. M., Wietschel, L., Thorenz, A., and Tuma, A. (2018a). Supply risks associated with lithium-ion battery materials. *J. Clean. Prod.* 172, 274–286. doi:10.1016/j.jclepro.2017.10.122

Helbig, C., Bradshaw, A. M., Wietschel, L., Thorenz, A., and Tuma, A. (2018b). Supply risks associated with lithium-ion battery materials. *J. Clean. Prod.* 172, 274–286. doi:10.1016/j.jclepro.2017.10.122

Herczog, A. (1985). Sodium ion conducting glasses for the sodium-sulfur battery. *J. Electrochem. Soc.* 132 (7), 1539–1545. doi:10.1149/1.2114161

Hibi, Y., Tanibata, N., Hayashi, A., and Tatsumisago, M. (2015). Preparation of sodium ion conducting Na_3PS_4-NaI glasses by a mechanochemical technique. *Solid State Ionics* 270, 6–9. Article. doi:10.1016/j.ssi.2014.11.024

Hill, R., Peretti, A., Small, L. J., Spoerke, E. D., and Cheng, Y.-T. (2023). Molten sodium penetration in NaSICON electrolytes at 0.1 A cm^{-2}. *ACS Appl. Energy Mater.* 6 (4), 2515–2523. doi:10.1021/acsaem.2c03944

Hill, R. C., Peretti, A. S., Maraschky, A. M., Small, L. J., Spoerke, E. D., and Cheng, Y.-T. (2024). Can a coating mitigate molten Na dendrite growth in NaSICON under high current density? *ACS Appl. Energy Mater.* 7, 810–819. doi:10.1021/acsaem.3c02994

Holzapfel, M., Wilde, D., Hupbauer, C., Ahlbrecht, K., and Berger, T. (2017). Medium-temperature molten sodium batteries with aqueous bromine and iodine cathodes. *Electrochimica Acta* 237, 12–21. doi:10.1016/j.electacta.2017.03.152

Hu, Y., Wen, Z., and Wu, X. (2014). Porous iron oxide coating on β″-alumina ceramics for Na-based batteries. *Solid State Ionics* 262, 133–137. doi:10.1016/j.ssi.2013.08.033

Hu, Y., Wen, Z., Wu, X., and Jin, J. (2012). Low-cost shape-control synthesis of porous carbon film on β″-alumina ceramics for Na-based battery application. *J. Power Sources* 219, 1–8. doi:10.1016/j.jpowsour.2012.07.025

Hu, Y., Wen, Z., Wu, X., and Lu, Y. (2013). Nickel nanowire network coating to alleviate interfacial polarization for Na-beta battery applications. *J. Power Sources* 240, 786–795. doi:10.1016/j.jpowsour.2013.04.056

International Energy Agency (2022). *World energy outlook 2022*. Paris: International Energy Agency.

Islam, M. A., Hasanuzzaman, M., Rahim, N. A., Nahar, A., and Hosenuzzaman, M. (2014). Global renewable energy-based electricity generation and smart grid system for energy security. *Sci. World J.* 2014, 1–13. doi:10.1155/2014/197136

Jebaselvi, G. A., and Paramasivam, S. (2013). Analysis on renewable energy systems. *Renew. Sustain. Energy Rev.* 28, 625–634. doi:10.1016/j.rser.2013.07.033

Jin, D., Choi, S., Jang, W., Soon, A., Kim, J., Moon, H., et al. (2019a). Bismuth islands for low-temperature sodium-beta alumina batteries. *ACS Appl. Mat. Interfaces* 11 (3), 2917–2924. doi:10.1021/acsami.8b13954

Jin, D., Lee, H. G., Choi, S., Kim, S., Lee, Y., Son, S., et al. (2019b). Sparked reduced graphene oxide for low-temperature sodium-beta alumina batteries. *Nano Lett.* 19 (12), 8811–8820. doi:10.1021/acs.nanolett.9b03646

Jin, M., Cheng, S., Yang, Z., Luo, Y., and Guo, Y. (2023). A novel high-voltage solid electrolyte of $Na_3B_{24}H_{23}$ for 4 V all-solid-state sodium battery. *Chem. Eng. J.* 455, 140904. doi:10.1016/j.cej.2022.140904

Jolley, A. G., Cohn, G., Hitz, G. T., and Wachsman, E. D. (2015a). Improving the ionic conductivity of NASICON through aliovalent cation substitution of $Na_3Zr_2Si_2PO_{12}$. *Ionics* 21 (11), 3031–3038. doi:10.1007/s11581-015-1498-8

Jolley, A. G., Taylor, D. D., Schreiber, N. J., and Wachsman, E. D. (2015b). Structural investigation of monoclinic-rhombohedral phase transition in $Na_3Zr_2Si_2PO_{12}$ and doped NaSICON. *J. Am. Ceram. Soc.* 98 (9), 2902–2907. doi:10.1111/jace.13692

Jonghe, L. C., Feldman, L., and Beuchele, A. (1981). Slow degradation and electron conduction in sodium/beta-aluminas. *J. Mat. Sci.* 16, 780–786. doi:10.1007/BF00552217

Jørgensen, M., Shea, P. T., Tomich, A. W., Varley, J. B., Bercx, M., Lovera, S., et al. (2020). Understanding superionic conductivity in lithium and sodium salts of weakly coordinating closo-hexahalocarbaborate anions. *Chem. Mat.* 32 (4), 1475–1487. doi:10.1021/acs.chemmater.9b04383

Jung, K., Chang, H.-J., Bonnett, J. F., Canfield, N. L., Sprenkle, V. L., and Li, G. (2018). An advanced Na-$NiCl_2$ battery using bi-layer (dense/micro-porous) β″-alumina solid-state electrolytes. *J. Power Sources* 396, 297–303. doi:10.1016/j.jpowsour.2018.06.039

Karabelli, D., Singh, S., Kiemel, S., Koller, J., Konarov, A., Stubhan, F., et al. (2020). Sodium-based batteries: in search of the best compromise between sustainability and maximization of electric performance. *Front. Energy Res.* 8. Review. doi:10.3389/fenrg.2020.605129

Kebede, A. A., Coosemans, T., Messagie, M., Jemal, T., Behabtu, H. A., Van Mierlo, J., et al. (2021). Techno-economic analysis of lithium-ion and lead-acid batteries in stationary energy storage application. *J. Energy Storage* 40, 102748. doi:10.1016/j.est.2021.102748

Keshri, S. R., Bodewad, V. V., Jagtap, A. A., Nasani, N., Balaji, S., Annapurna, K., et al. (2020). Influence of NaF on the ionic conductivity of sodium aluminophosphate glass electrolytes. *Mater. Lett.* 271, 127763. doi:10.1016/j.matlet.2020.127763

Keshri, S. R., Ganisetti, S., Kumar, R., Gaddam, A., Illath, K., Ajithkumar, T. G., et al. (2021). Ionic conductivity of $Na_3Al_2P_3O_{12}$ glass electrolytes—role of charge compensators. *Inorg. Chem.* 60 (17), 12893–12905. doi:10.1021/acs.inorgchem.1c01280

Keshri, S. R., Mandal, I., Ganisetti, S., Kasimuthumaniyan, S., Kumar, R., Gaddam, A., et al. (2022). Elucidating the influence of structure and Ag+-Na+ ion-exchange on crack-resistance and ionic conductivity of $Na_3Al_{1.8}Si_{1.65}P_{1.8}O_{12}$ glass electrolyte. *Acta Mater.* 227, 117745. doi:10.1016/j.actamat.2022.117745

Kim, H., Boysen, D. A., Newhouse, J. M., Spatocco, B. L., Chung, B., Burke, P. J., et al. (2013). Liquid metal batteries: past, present, and future. *Chem. Rev.* 113 (3), 2075–2099. doi:10.1021/cr300205k

Kim, H.-T., Kim, S.-I., Choi, H.-L., Park, W.-I., and Kim, C.-s. (2015b). Effect of Zn/NaCl ratios on the charge/discharge performance in Na-$ZnCl_2$ battery. *J. Korean Cryst. Growth Cryst. Technol.* 25 (2), 74–79. doi:10.6111/jkcgct.2015.25.2.074

Kim, I., Park, J.-Y., Kim, C. H., Park, J.-W., Ahn, J.-P., Ahn, J.-H., et al. (2016). A room temperature Na/S battery using a β″ alumina solid electrolyte separator, tetraethylene glycol dimethyl ether electrolyte, and a S/C composite cathode. *J. Power Sources* 301, 332–337. doi:10.1016/j.jpowsour.2015.09.120

Kim, J., Jo, S. H., Bhavaraju, S., Eccleston, A., and Kang, S. O. (2015a). Low temperature performance of sodium–nickel chloride batteries with NaSICON solid electrolyte. *J. Electroanal. Chem.* 759, 201–206. doi:10.1016/j.jelechem.2015.11.022

Kim, K., Mundy, J., and Chen, W. (1979). Diffusion and ionic conductivity in sodium beta alumina. *J. Phys. Chem. Solids* 40 (10), 743–755. doi:10.1016/0022-3697(79)90157-4

Kim, M., Ahn, C.-W., Hahn, B.-D., Jung, K., Park, Y.-C., Cho, N.-u., et al. (2017). Effects of Ni particle morphology on cell performance of Na/$NiCl_2$ battery. *Metals Mater. Int.* 23 (6), 1234–1240. doi:10.1007/s12540-017-7062-5

Kim, S. M., Lee, S. M., Jung, K., Park, Y. C., Cho, N. u., Choi, J. H., et al. (2015c). Influence of carbon coating on beta-alumina membrane for sodium–nickel chloride battery. *Bull. Korean Chem. Soc.* 36 (12), 2869–2874. doi:10.1002/bkcs.10584

Koduru, H. K., Iliev, M., Kondamareddy, K., Karashanova, D., Vlakhov, T., Zhao, X.-Z., et al. (2016). Investigations on Poly (ethylene oxide)(PEO)-blend based solid polymer electrolytes for sodium ion batteries. *J. Phys. Conf. Ser.* 764, 012006. doi:10.1088/1742-6596/764/1/012006

Koganei, K., Oyama, T., Inada, M., Enomoto, N., and Hayashi, K. (2014). C-axis oriented β ″-alumina ceramics with anisotropic ionic conductivity prepared by spark plasma sintering. *Solid State Ionics* 267, 22–26. doi:10.1016/j.ssi.2014.09.003

Kohler, H., and Schulz, H. (1985). NASICON solid electrolytes part I: the Na^+-diffusion path and its relation to the structure. *Mater. Res. Bull.* 20 (12), 1461–1471. doi:10.1016/0025-5408(85)90164-3

Kohler, H., Schulz, H., and Melnikov, O. (1983). Composition and conduction mechanism of the NASICON structure X-ray diffraction study on two crystals at different temperatures. *Mater. Res. Bull.* 18 (9), 1143–1152. doi:10.1016/0025-5408(83)90158-7

Kosowatz, J. (2018). Energy storage smooths the duck curve. *Mech. Eng.* 140 (06), 30–35. doi:10.1115/1.2018-JUN-1

Kreps, B. H. (2020). The rising costs of fossil-fuel extraction: an energy crisis that will not go away. *Am. J. Econ. Sociol.* 79 (3), 695–717. doi:10.1111/ajes.12336

Kreuer, K. D., and Warhus, U. (1986). NASICON solid electrolytes: Part IV Chemical durability. *Mater. Res. Bull.* 21 (3), 357–363. doi:10.1016/0025-5408(86)90193-5

Kumar, S., Ding, W., Hoffmann, R., Sieuw, L., Heinz, M. V., Weber, N., et al. (2023). $AlCl_3$-NaCl-$ZnCl_2$ secondary electrolyte in next-generation ZEBRA (Na-$ZnCl_2$) battery. *Batteries* 9 (8), 401. doi:10.3390/batteries9080401

Kummer, J. T. (1972). β-Alumina electrolytes. *Prog. Solid State Chem.* 7, 141–175. doi:10.1016/0079-6786(72)90007-6

Kummer, J. T., and Weber, N. (1968). A sodium-sulfur secondary battery. *Sae Trans.*, 1003–1028. doi:10.4271/670179

Kweon, K. E., Varley, J. B., Shea, P., Adelstein, N., Mehta, P., Heo, T. W., et al. (2017). Structural, chemical, and dynamical frustration: origins of superionic conductivity in closo-borate solid electrolytes. *Chem. Mat.* 29 (21), 9142–9153. doi:10.1021/acs.chemmater.7b02902

Lai, H., Wang, J., Cai, M., Song, Z., Gao, X., Wu, X., et al. (2022). Double-functional 3D cross-linking carbon fiber with Sn particle coating layer for improving interfacial performance of Na-β ″-Al_2O_3 batteries. *Chem. Eng. J.* 433, 133545. doi:10.1016/j.cej.2021.133545

Lan, T., Graeber, G., Sieuw, L., Svaluto-Ferro, E., Vagliani, F., Basso, D., et al. (2023). Planar sodium-nickel chloride batteries with high areal capacity for sustainable energy storage. *Adv. Funct. Mater.* 33 (33), 2302040. doi:10.1002/adfm.202302040

Landmann, D., Graeber, G., Heinz, M. V. F., Haussener, S., and Battaglia, C. (2020). Sodium plating and stripping from Na-β″-alumina ceramics beyond 1000 mA/cm^2. *Mater. Today Energy* 18, 100515. doi:10.1016/J.MTENER.2020.100515

Lazar, M., Kmiec, S., Joyce, A., and Martin, S. W. (2020). Investigations into reactions between sodium metal and $Na_3PS_{4-x}O_x$ solid-state electrolytes: enhanced stability of the Na_3PS_3O solid-state electrolyte. *ACS Appl. energy Mater.* 3, 11559–11569. doi:10.1021/acsaem.0c00914

Lee, D.-H., Lee, S.-T., Kim, J.-S., and Lim, S.-K. (2017). Analysis of properties of partially stabilized zirconia-doped Na^+-beta-alumina prepared by calcining-cum-sintering process. *Mater. Res. Bull.* 96, 143–148. doi:10.1016/j.materresbull.2017.05.003

Lee, R. Y., Percival, S. J., and Small, L. J. (2021). Electrochemical modeling of iodide oxidation in metal-halide molten salts. *J. Electrochem. Soc.* 168 (12), 126511. doi:10.1149/1945-7111/ac3e7a

Lee, Y., Kim, H.-J., Byun, D.-J., Cho, K.-K., Ahn, J.-H., and Kim, C.-S. (2019). Electrochemically activated Na–$ZnCl_2$ battery using a carbon matrix in the cathode compartment. *J. Power Sources* 440, 227110. doi:10.1016/j.jpowsour.2019.227110

Leng, H., Huang, J., Nie, J., and Luo, J. (2018). Cold sintering and ionic conductivities of $Na_{3.256}Mg_{0.128}Zr_{1.872}Si_2PO_{12}$ solid electrolytes. *J. Power Sources* 391, 170–179. doi:10.1016/j.jpowsour.2018.04.067

Leng, H. Y., Nie, J. Y., and Luo, J. (2019). Combining cold sintering and Bi_2O_3-Activated liquid-phase sintering to fabricate high-conductivity Mg-doped NASICON at reduced temperatures. *J. Materiomics* 5 (2), 237–246. Article. doi:10.1016/j.jmat.2019.02.005

Li, C., Jiang, S., Lv, J.-w., and Zheng, T. (2015b). Ionic conductivities of Na–Ge–P glass ceramics as solid electrolyte. *J. Alloys Compd.* 633, 246–249. doi:10.1016/j.jallcom.2014.12.183

Li, G., Lu, X., Kim, J. Y., Lemmon, J. P., and Sprenkle, V. L. (2013). Cell degradation of a Na–$NiCl_2$ (ZEBRA) battery. *J. Mat. Chem. A* 1 (47), 14935. doi:10.1039/c3ta13644b

Li, G., Lu, X., Kim, J. Y., Lemmon, J. P., and Sprenkle, V. L. (2014). Improved cycling behavior of ZEBRA battery operated at intermediate temperature of 175 °C. *J. Power Sources* 249, 414–417. doi:10.1016/j.jpowsour.2013.10.110

Li, G., Lu, X., Kim, J. Y., Meinhardt, K. D., Chang, H. J., Canfield, N. L., et al. (2016a). Advanced intermediate temperature sodium–nickel chloride batteries with ultra-high energy density. *Nat. Commun.* 7 (1), 10683. doi:10.1038/ncomms10683

Li, G., Lu, X., Kim, J. Y., Viswanathan, V. V., Meinhardt, K. D., Engelhard, M. H., et al. (2015a). An advanced Na–$FeCl_2$ ZEBRA battery for stationary energy storage application. *Adv. Energy Mater.* 5 (12), 1500357. doi:10.1002/aenm.201500357

Li, H., Fan, H., Zhang, J., Wen, Y., Chen, G., Zhu, Y., et al. (2019). Sintering behavior and properties of lithium stabilized sodium β'' - alumina ceramics with YSZ addition. *Ceram. Int.* 45 (6), 6744–6752. doi:10.1016/j.ceramint.2018.12.165

Li, H., Yin, H., Wang, K., Cheng, S., Jiang, K., and Sadoway, D. R. (2016b). Liquid metal electrodes for energy storage batteries. *Adv. Energy Mater.* 6 (14), 1600483. doi:10.1002/aenm.201600483

Li, K., Ma, M., Yang, Y., Liang, S., and Zhang, X. (2021b). Preparation of β"-Al_2O_3 electrolytes by freeze-drying and SPS. *Ceram. Int.* 47 (11), 15017–15022. doi:10.1016/j.ceramint.2021.02.057

Li, K., Yang, Y., Zhang, X., and Liang, S. (2020b). Highly oriented β ″-alumina ceramics with excellent ionic conductivity and mechanical performance obtained by spark plasma sintering technique. *J. Mat. Sci.* 55, 8435–8443. doi:10.1007/s10853-020-04423-x

Li, M. M., Tripathi, S., Polikarpov, E., Canfield, N. L., Han, K. S., Weller, J. M., et al. (2022). Interfacial engineering with a nanoparticle-decorated porous carbon structure on β″-alumina solid-state electrolytes for molten sodium batteries. *ACS Appl. Mat. Interfaces* 14 (22), 25534–25544. doi:10.1021/acsami.2c05245

Li, Y., Shi, L., Gao, X., Wang, J., Hu, Y., Wu, X., et al. (2021a). Constructing a charged-state Na-$NiCl_2$ battery with $NiCl_2$/graphene aerogel composite as cathode. *Chem. Eng. J.* 421, 127853. doi:10.1016/j.cej.2020.127853

Li, Y., Wu, X., Wang, J., Gao, X., Hu, Y., and Wen, Z. (2020a). Ni-less cathode with 3D free-standing conductive network for planar Na-$NiCl_2$ batteries. *Chem. Eng. J.* 387, 124059. doi:10.1016/j.cej.2020.124059

Liu, C., Shamie, J. S., Shaw, L. L., and Sprenkle, V. L. (2016). An ambient temperature molten sodium–vanadium battery with aqueous flowing catholyte. *ACS Appl. Mat. Interfaces* 8 (2), 1545–1552. doi:10.1021/acsami.5b11503

Liu, Z., Chen, J., Wang, X., Wang, Y., Wang, D., and Mao, Z. (2020). Synthesis and characterization of high ionic-conductive sodium beta-alumina solid electrolyte derived from boehmite. *J. Mat. Sci. Mat. Electron.* 31 (20), 17670–17678. doi:10.1007/s10854-020-04321-7

Long Duration Energy Storage Council (2022). *The journey to net-zero: an action plan to unlock a secure, net-zero power system*. Long Duration Energy Storage Council.

Lu, J., Tang, J., Shan, R., Li, G., Rao, P., and Zhang, N. (2023). Spatiotemporal analysis of the future carbon footprint of solar electricity in the United States by a dynamic life cycle assessment. *iScience* 26 (3), 106188. doi:10.1016/j.isci.2023.106188

Lu, X., Chang, H. J., Bonnett, J. F., Canfield, N. L., Jung, K., Sprenkle, V. L., et al. (2017). Effect of cathode thickness on the performance of planar Na-$NiCl_2$ battery. *J. Power Sources* 365, 456–462. doi:10.1016/j.jpowsour.2017.07.029

Lu, X., Chang, H. J., Bonnett, J. F., Canfield, N. L., Jung, K., Sprenkle, V. L., et al. (2018). An intermediate-temperature high-performance Na–$ZnCl_2$ battery. *ACS Omega* 3 (11), 15702–15708. doi:10.1021/acsomega.8b02112

Lu, X., Kirby, B. W., Xu, W., Li, G., Kim, J. Y., Lemmon, J. P., et al. (2013b). Advanced intermediate-temperature Na–S battery. *Energy Environ. Sci.* 6 (1), 299–306. doi:10.1039/C2EE23606K

Lu, X., Lemmon, J. P., Sprenkle, V., and Yang, Z. (2010a). Sodium-beta alumina batteries: status and challenges. *JOM* 62 (9), 31–36. doi:10.1007/s11837-010-0132-5

Lu, X., Li, G., Kim, J. Y., Lemmon, J. P., Sprenkle, V. L., and Yang, Z. (2012). The effects of temperature on the electrochemical performance of sodium–nickel chloride batteries. *J. Power Sources* 215, 288–295. doi:10.1016/j.jpowsour.2012.05.020

Lu, X., Li, G., Kim, J. Y., Lemmon, J. P., Sprenkle, V. L., and Yang, Z. (2013c). A novel low-cost sodium–zinc chloride battery. *Energy & Environ. Sci.* 6 (6), 1837. doi:10.1039/c3ee24244g

Lu, X., Li, G., Kim, J. Y., Mei, D., Lemmon, J. P., Sprenkle, V. L., et al. (2014). Liquid-metal electrode to enable ultra-low temperature sodium–beta alumina batteries for renewable energy storage. *Nat. Commun.* 5 (1), 4578. doi:10.1038/ncomms5578

Lu, X., Li, G., Kim, J. Y., Meinhardt, K. D., and Sprenkle, V. L. (2015). Enhanced sintering of β″-Al_2O_3/YSZ with the sintering aids of TiO_2 and MnO_2. *J. Power Sources* 295, 167–174. doi:10.1016/j.jpowsour.2015.06.147

Lu, X., Xia, G., Lemmon, J. P., and Yang, Z. (2010b). Advanced materials for sodium-beta alumina batteries: status, challenges and perspectives. *J. Power Sources* 195 (9), 2431–2442. doi:10.1016/j.jpowsour.2009.11.120

Lu, X. C., Lemmon, J. P., Kim, J. Y., Sprenkle, V. L., and Yang, Z. G. (2013a). High energy density Na-S/$NiCl_2$ hybrid battery. *J. Power Sources* 224, 312–316. doi:10.1016/j.jpowsour.2012.09.108

Mali, A., and Petric, A. (2012). Synthesis of sodium β″-alumina powder by sol–gel combustion. *J. Eur. Ceram. Soc.* 32 (6), 1229–1234. doi:10.1016/j.jeurceramsoc.2011.11.004

Manchgesang, W., Wagner, D., Motylenko, M., Schilm, J., Rafaja, D., and Meyer, D. C. (2018). Influence of the glass-ceramic synthesis route on the ionicconductivity of the sodium solid electrolyte Na_2O-Y_2O_3-SiO_2 (NYS). *Acta Crystallogr. Sect. A* 74, E286. Meeting Abstract. doi:10.1107/s2053273318090861

Maraschky, A. M., Meyerson, M. L., Percival, S. J., Lowry, D. R., Meserole, S., Williard, J. N., et al. (2023a). Impact of catholyte lewis acidity at the molten salt–NaSICON interface in low-temperature molten sodium batteries. *J. Phys. Chem. C* 127 (3), 1293–1302. doi:10.1021/acs.jpcc.2c06240

Maraschky, A. M., Percival, S. J., Lee, R. Y., Meyerson, M. L., Peretti, A. S., Spoerke, E. D., et al. (2023b). Electrode blocking due to redox reactions in aluminum chloride-sodium iodide molten salts. *J. Electrochem. Soc.* 170 (6), 066504. doi:10.1149/1945-7111/acd874

Mekhilef, S., Saidur, R., and Safari, A. (2011). A review on solar energy use in industries. *Renew. Sustain. Energy Rev.* 15 (4), 1777–1790. doi:10.1016/j.rser.2010.12.018

Miao, R. J., Cao, X. G., Wang, W. G., and Zhang, H. Y. (2021). Influence of Bi_2O_3 additive on the electrochemical performance of $Na_{3.1}$ $Y_{0.1}Zr_{1.9}Si_2PO_{12}$ inorganic solid electrolyte. *Ceram. Int.* 47 (12), 17455–17462. Article. doi:10.1016/j.ceramint.2021.03.062

Moran, E. F., Lopez, M. C., Moore, N., Müller, N., and Hyndman, D. W. (2018). Sustainable hydropower in the 21st century. *Proc. Natl. Acad. Sci.* 115 (47), 11891–11898. doi:10.1073/pnas.1809426115

Mortalò, C., Rosa, R., Veronesi, P., Fasolin, S., Zin, V., Deambrosis, S. M., et al. (2020). Microwave assisted sintering of Na-β''-Al_2O_3 in single mode cavities: insights in the use of 2450 MHz frequency and preliminary experiments at 5800 MHz. *Ceram. Int.* 46 (18), 28767–28777. Part A). doi:10.1016/j.ceramint.2020.08.039

Nagaura, T. (1990). Lithium ion rechargeable battery. *Prog. Batter. Sol. Cells* 9, 209.

NAS Batteries (2023). Designed for stationary energy storage. Available at: https://www.basf.com/global/en/who-we-are/organization/group-companies/BASF-Stationary-Energy-Storage-GmbH/designed-for-stationary-energy-storage.html (Accessed December 30, 2023).

Nasu, A., Inaoka, T., Tsuji, F., Motohashi, K., Sakuda, A., Tatsumisago, M., et al. (2022). Formation of passivate interphases by Na_3BS_3-glass solid electrolytes in all-solid-state sodium-metal batteries. *ACS Appl. Mat. Interfaces* 14 (21), 24480–24485. doi:10.1021/acsami.2c05090

National Research Council (2012). *The role of the chemical sciences in finding alternatives to critical resources: a workshop summary*. Washington (DC): National Academies Press.

NGL-Insulator (2023). About NAS batteries. https://www.ngk-insulators.com/en/product/nas-about.html (Accessed December 30, 2023).

Ni, Y., Zheng, R., Tan, X., Yue, W., Lv, P., Yang, J., et al. (2015). A fluorophosphate glass–ceramic electrolyte with superior ionic conductivity and stability for Na-ion batteries. *J. Mat. Chem. A* 3 (34), 17558–17562. doi:10.1039/c5ta03030g

Nieto-Muñoz, A. M., Ortiz-Mosquera, J. F., and Rodrigues, A. C. M. (2019). Novel sodium superionic conductor of the $Na_{1+y}Ti_2Si_yP_{3-y}O_{12}$ series for application as solid electrolyte. *Electrochimica Acta* 319, 922–932. doi:10.1016/j.electacta.2019.07.032

Nieto-Muñoz, A. M., Ortiz-Mosquera, J. F., and Rodrigues, A. C. M. (2020). The impact of heat-treatment protocol on the grain size and ionic conductivity of NASICON glass-ceramics. *J. Eur. Ceram. Soc.* 40 (15), 5634–5645. doi:10.1016/j.jeurceramsoc.2020.05.026

Nikiforidis, G., Jongerden, G. J., Jongerden, E. F., Van De Sanden, M. C. M., and Tsampas, M. N. (2019). An electrochemical study on the cathode of the intermediate temperature tubular sodium-sulfur (NaS) battery. *J. Electrochem. Soc.* 166 (2), A135–A142. doi:10.1149/2.0491902jes

Nimah, Y. L., Cheng, M.-Y., Cheng, J. H., Rick, J., and Hwang, B.-J. (2015). Solid-state polymer nanocomposite electrolyte of TiO_2/PEO/$NaClO_4$ for sodium ion batteries. *J. Power Sources* 278, 375–381. doi:10.1016/j.jpowsour.2014.11.047

Niu, C., Ji, L., Chen, Y., Ma, S., Zhang, Y., Liu, X., et al. (2021). Low-melting-point ionic liquid electrolyte for an intermediate-temperature sodium–copper chloride battery. *Energy & Fuels* 35 (15), 12538–12545. doi:10.1021/acs.energyfuels.1c00833

Niu, C., Zhang, Y., Ma, S., Wan, Y., Yang, H., and Liu, X. (2019). An intermediate temperature sodium copper chloride battery using ionic liquid electrolyte and its degradation mechanism. *Ionics* 25, 4189–4196. doi:10.1007/s11581-019-03003-7

Noi, K., Suzuki, K., Tanibata, N., Hayashi, A., and Tatsumisago, M. (2018). Liquid-phase sintering of highly Na^+ ion conducting $Na_3Zr_2Si_2PO_{12}$ ceramics using Na_3BO_3 additive. *J. Am. Ceram. Soc.* 101 (3), 1255–1265. Article. doi:10.1111/jace.15288

Nose, M., Kato, A., Sakuda, A., Hayashi, A., and Tatsumisago, M. (2015). Evaluation of mechanical properties of Na_2S–P_2S_5 sulfide glass electrolytes. *J. Mat. Chem. A* 3 (44), 22061–22065. doi:10.1039/C5TA05590C

Oh, J. A. S., He, L. C., Plewa, A., Morita, M., Zhao, Y., Sakamoto, T., et al. (2019). Composite NASICON ($Na_3Zr_2Si_2PO_{12}$) solid-state electrolyte with enhanced Na^+ ionic conductivity: effect of liquid phase sintering. *ACS Appl. Mat. Interfaces* 11 (43), 40125–40133. Article. doi:10.1021/acsami.9b14986

Ohi, J. M. (1992). *Environmental, health, and safety issues of sodium-sulfur batteries for electric and hybrid vehicles*. Golden, CO (United States): National Renewable Energy Lab.

Olson, M., Wheaton, J., Okkema, M., Oldham, N., and Martin, S. W. (2023). Optimized thin film processing of sodium mixed oxy-sulfide-nitride glassy solid electrolytes for all-solid-state batteries. *ACS Appl. energy Mater.* 6 (11), 5842–5855. doi:10.1021/acsaem.3c00294

Park, H. C., Lee, Y. B., Lee, S. G., Lee, C. H., Kim, J. K., Hong, S. S., et al. (2005). Synthesis of beta-alumina powders by microwave heating from solution-derived precipitates. *Ceram. Int.* 31 (2), 293–296. doi:10.1016/j.ceramint.2004.05.019

Parthasarathy, P., Weber, N., and Virkar, A. V. (2007). High temperature sodium-zinc chloride batteries with sodium beta-alumina solid electrolyte. *ECS Trans.* 6 (14), 67–76. doi:10.1149/1.2811944

Pauling, L. (1927). The sizes of ions and the structure of ionic crystals. *J. Am. Chem. Soc.* 49 (3), 765–790. doi:10.1021/ja01402a019

Peled, E., Golodnitsky, D., Hadar, R., Mazor, H., Goor, M., and Burstein, L. (2013). Challenges and obstacles in the development of sodium–air batteries. *J. Power Sources* 244, 771–776. doi:10.1016/j.jpowsour.2013.01.177

Percival, S. J., Lee, R. Y., Gross, M. M., Peretti, A. S., Small, L. J., and Spoerke, E. D. (2021). Electrochemistry of the NaI-$AlBr_3$ molten salt system: a redox-active, low-temperature molten salt electrolyte. *J. Electrochem. Soc.* 168 (3), 036510. doi:10.1149/1945-7111/abebae

Percival, S. J., Small, L. J., and Spoerke, E. D. (2018). Electrochemistry of the NaI-$AlCl_3$ molten salt system for use as catholyte in sodium metal batteries. *J. Electrochem. Soc.* 165 (14), A3531–A3536. doi:10.1149/2.1191814jes

Pereirinha, P. G., González, M., Carrilero, I., Anseán, D., Alonso, J., and Viera, J. C. (2018). Main trends and challenges in road transportation electrification. *Transp. Res. Procedia* 33, 235–242. doi:10.1016/j.trpro.2018.10.096

Perera, F. P. (2017). Multiple threats to child health from fossil fuel combustion: impacts of air pollution and climate change. *Environ. Health Perspect.* 125 (2), 141–148. doi:10.1289/ehp299

Qiao, L., Judez, X., Rojo, T., Armand, M., and Zhang, H. (2020). Review—polymer electrolytes for sodium batteries. *J. Electrochem. Soc.* 167 (7), 070534. doi:10.1149/1945-7111/ab7aa0

Rahman, M. M., Oni, A. O., Gemechu, E., and Kumar, A. (2020). Assessment of energy storage technologies: a review. *Energy Convers. Manag.* 223, 113295. doi:10.1016/j.enconman.2020.113295

Rajagopalan, R., Zhang, Z., Tang, Y., Jia, C., Ji, X., and Wang, H. (2021). Understanding crystal structures, ion diffusion mechanisms and sodium storage behaviors of NASICON materials. *Energy Storage Mater.* 34, 171–193. doi:10.1016/j.ensm.2020.09.007

Ray, A. K., and Subbarao, E. C. (1975). Synthesis of sodium β and β″ alumina. *Mater. Res. Bull.* 10 (6), 583–590. doi:10.1016/0025-5408(75)90186-5

Reed, D., Coffey, G., Mast, E., Canfield, N., Mansurov, J., Lu, X., et al. (2013). Wetting of sodium on β ″-Al_2O_3/YSZ composites for low temperature planar sodium-metal halide batteries. *J. Power Sources* 227, 94–100. doi:10.1016/j.jpowsour.2012.11.034

Richman, R. H., and Tennenhouse, G. J. (1975). A model for degradation of ceramic electrolytes in Na-S batteries. *J. Am. Ceram. Soc.* 58, 63–67. doi:10.1111/J.1151-2916.1975.TB18986.X

Sakaebe, H. (2014). "ZEBRA batteries," in *Encyclopedia of applied electrochemistry*. Editors G Kreysa, K Ota, and R F Savinell (New York: Springer), 2165–2169.

Samiee, M., Radhakrishnan, B., Rice, Z., Deng, Z., Meng, Y. S., Ong, S. P., et al. (2017). Divalent-doped $Na_3Zr_2Si_2PO_{12}$ natrium superionic conductor: improving the ionic conductivity via simultaneously optimizing the phase and chemistry of the primary and secondary phases. *J. Power Sources* 347, 229–237. doi:10.1016/j.jpowsour.2017.02.042

Schmid, H., De Jonghe, L. C., and Cameron, C. (1982). Chemical stability of nasicon. *Solid State Ionics* 6, 57–63. doi:10.1016/0167-2738(82)90096-0

Shamie, J. S., Liu, C., Shaw, L. L., and Sprenkle, V. L. (2015). Room temperature, hybrid sodium-based flow batteries with multi-electron transfer redox reactions. *Sci. Rep.* 5 (1), 11215. doi:10.1038/srep11215

Shao, B., Huang, Y., and Han, F. (2023). Electronic conductivity of lithium solid electrolytes. *Adv. Energy Mater.* 13 (16), 2204098. doi:10.1002/aenm.202204098

Shao, Y., Zhong, G., Lu, Y., Liu, L., Zhao, C., Zhang, Q., et al. (2019). A novel NASICON-based glass-ceramic composite electrolyte with enhanced Na-ion conductivity. *Energy Storage Mater.* 23, 514–521. doi:10.1016/j.ensm.2019.04.009

Shimizu, Y., Azuma, Y., and Michishita, S. (1997). Sol–gel synthesis of NASICON discs from aqueous solution. *J. Mat. Chem.* 7 (8), 1457–1460. doi:10.1039/a608364a

Sieuw, L., Lan, T., Svaluto-Ferro, E., Vagliani, F., Kumar, S., Ding, W., et al. (2024). Influence of precursor morphology and cathode processing on performance and cycle life of sodium-zinc chloride (Na-$ZnCl_2$) battery cells. *Energy Storage Mater.* 64, 103077. doi:10.1016/j.ensm.2023.103077

Small, L. J., Eccleston, A., Lamb, J., Read, A. C., Robins, M., Meaders, T., et al. (2017). Next generation molten NaI batteries for grid scale energy storage. *J. Power Sources* 360, 569–574. doi:10.1016/j.jpowsour.2017.06.038

Solstice (2023). Solstice Available at: https://www.solstice-battery.eu/about/ (Accessed December-30-2023).

Sozak, M., Nazarenus, T., Exner, J., Kita, J., and Moos, R. (2023). Room temperature manufacture of dense NaSICON solid electrolyte films for all-solid-state-sodium batteries. *J. Mat. Sci.* 58 (24), 10108–10119. doi:10.1007/s10853-023-08642-w

Spatocco, B. L., Ouchi, T., Lambotte, G., Burke, P. J., and Sadoway, D. R. (2015). Low-temperature molten salt electrolytes for membrane-free sodium metal batteries. *J. Electrochem. Soc.* 162 (14), A2729–A2736. doi:10.1149/2.0441514jes

Spoerke, E. D., Durvasulu, V., and Balliet, H. (2030). Sodium batteries technology strategy assesssment. *Storage Innov.*, 2023.

Stevens, R., and Binner, J. G. P. (1984). Structure, properties and production of β-alumina. *J. Mat. Sci.* 19 (3), 695–715. doi:10.1007/bf00540440

Sudworth, J. L. (2001). The sodium/nickel chloride (ZEBRA) battery. *J. Power Sources* 100, 149–163. doi:10.1016/S0378-7753(01)00891-6

Sudworth, J. L., and Tilley, A. R. (1986). *Sodium sulphur battery*. London: Chapman & Hall.

Sundar, G., Suman, G., Kumar, K., Dutta, D., and Rao, R. (2019). Investigation on the applicability of high Na-ion conducting $Na_{3+x}[Zr_xSc_{2-x}(PO_4)_3]$ glass-ceramic electrolyte for use in safer Na-ion batteries. *J. Phys. Chem. Solids* 126, 209–218. doi:10.1016/j.jpcs.2018.11.016

Susman, S., Delbecq, C. J., McMillan, J. A., and Roche, M. F. (1983). NASIGLAS: a new vitreous electrolyte. *Solid State Ionics* 9-10, 667–673. doi:10.1016/0167-2738(83)90312-0

Suzuki, K., Noi, K., Hayashi, A., and Tatsumisago, M. (2018). Low temperature sintering of $Na_{1+x}Zr_2Si_xP_{3-x}O_{12}$ by the addition of Na_3BO_3. *Scr. Mater.* 145, 67–70. Article. doi:10.1016/j.scriptamat.2017.10.010

Tang, W. S., Dimitrievska, M., Stavila, V., Zhou, W., Wu, H., Talin, A. A., et al. (2017). Order–disorder transitions and superionic conductivity in the sodium nido-undeca (carba) borates. *Chem. Mat.* 29 (24), 10496–10509. doi:10.1021/acs.chemmater.7b04332

Tang, W. S., Yoshida, K., Soloninin, A. V., Skoryunov, R. V., Babanova, O. A., Skripov, A. V., et al. (2016). Stabilizing superionic-conducting structures via mixed-anion solid solutions of monocarba-closo-borate salts. *ACS Energy Lett.* 1 (4), 659–664. doi:10.1021/acsenergylett.6b00310

Tanibata, N., Noi, K., Hayashi, A., Kitamura, N., Idemoto, Y., and Tatsumisago, M. (2014). X-ray crystal structure analysis of sodium-ion conductivity in $94Na_3PS_4{\cdot}6Na_4SiS_4$ glass-ceramic electrolytes. *ChemElectroChem* 1 (7), 1130–1132. doi:10.1002/celc.201402016

Tanibata, N., Noi, K., Hayashi, A., and Tatsumisago, M. (2018). Preparation and characterization of Na_3PS_4–Na_4GeS_4 glass and glass-ceramic electrolytes. *Solid State Ionics* 320, 193–198. doi:10.1016/j.ssi.2018.02.042

Tatsumisago, M., and Hayashi, A. (2014). Sulfide glass-ceramic electrolytes for all-solid-state lithium and sodium batteries. *Int. J. Appl. Glass Sci.* 5 (3), 226–235. doi:10.1111/ijag.12084

Trickett, D. (1998). *Current status of health and safety issues of sodium/metal chloride (ZEBRA) batteries*. Golden, CO (United States): National Renewable Energy Lab.

Tsai, C. L., and Hong, H. Y. P. (1983). Investigation of phases and stability of solid electrolytes in the NASICON system. *Mater. Res. Bull.* 18 (11), 1399–1407. doi:10.1016/0025-5408(83)90048-X

Tsuji, F., Nasu, A., Hotehama, C., Sakuda, A., Tatsumisago, M., and Hayashi, A. (2021). Preparation and characterization of sodium-ion conductive Na_3BS_3 glass and glass–ceramic electrolytes. *Mat. Adv.* 2 (5), 1676–1682. doi:10.1039/d0ma00777c

Tsuji, F., Tanibata, N., Sakuda, A., Hayashi, A., and Tatsumisago, M. (2018). Preparation of sodium ion conductive $Na_{10}GeP_2S_{12}$ glass-ceramic electrolytes. *Chem. Lett.* 47 (1), 13–15. Article. doi:10.1246/cl.170836

Tu, X., Chu, Y., and Ma, C. (2010). New ternary molten salt electrolyte based on alkali metal triflates. *Ionics* 16 (1), 81–84. doi:10.1007/s11581-009-0390-9

Udovic, T. J., Matsuo, M., Unemoto, A., Verdal, N., Stavila, V., Skripov, A. V., et al. (2014). Sodium superionic conduction in $Na_2B_{12}H_{12}$. *Chem. Commun.* 50 (28), 3750–3752. doi:10.1039/C3CC49805K

van Zyl, A., Thackeray, M. M., Duncan, G. K., Kingon, A. I., and Heckroodt, R. O. (1993). The synthesis of beta alumina from aluminium hydroxide and oxyhydroxide precursors. *Mater. Res. Bull.* 28 (2), 145–157. doi:10.1016/0025-5408(93)90083-P

Virkar, A. (2008). *A high temperature electrochemical energy storage system based on sodium beta-alumina solid electrolyte (Base)*. Salt Lake City, UT (United States): Univ. of Utah.

Virkar, A. V., and Viswanathan, L. (1983). A three-dimensional approach to the electrolytic degradation of solid electrolytes. *J. Mat. Sci.* 18 (4), 1202–1212. doi:10.1007/bf00551990

Viswanathan, L., and Virkar, A. V. (1982). Wetting characteristics of sodium on β″-alumina and on nasicon. *J. Mat. Sci.* 17, 753–759. doi:10.1007/BF00540372

Wang, D., Hwang, J., Chen, C. Y., Kubota, K., Matsumoto, K., and Hagiwara, R. (2021). A β-alumina/inorganic ionic liquid dual electrolyte for intermediate-temperature sodium–sulfur batteries. *Adv. Funct. Mater.* 31 (48), 9. doi:10.1002/adfm.202105524

Wang, N., Wang, Y., Bai, Z., Fang, Z., Zhang, X., Xu, Z., et al. (2020b). High-performance room-temperature sodium–sulfur battery enabled by electrocatalytic sodium polysulfides full conversion. *Energy & Environ. Sci.* 13 (2), 562–570. doi:10.1039/c9ee03251g

Wang, X., Chen, J., Mao, Z., and Wang, D. (2022). Effective resistance to dendrite growth of NASICON solid electrolyte with lower electronic conductivity. *Chem. Eng. J.* 427, 130899. doi:10.1016/j.cej.2021.130899

Wang, Y., Zhou, D., Palomares, V., Shanmukaraj, D., Sun, B., Tang, X., et al. (2020a). Revitalising sodium–sulfur batteries for non-high-temperature operation: a crucial review. *Energy & Environ. Sci.* 13 (11), 3848–3879. doi:10.1039/d0ee02203a

Warhus, U., Maier, J., and Rabenau, A. (1988). Thermodynamics of NASICON ($Na_{1+x}Zr_2Si_xP_{3-x}O_{12}$). *J. Solid State Chem.* 72 (1), 113–125. doi:10.1016/0022-4596(88)90014-X

Wei, M., McMillan, C. A., and de la Rue du Can, S. (2019). Electrification of industry: potential, challenges and outlook. *Curr. Sustainable/Renewable Energy Rep.* 6 (4), 140–148. doi:10.1007/s40518-019-00136-1

Wei, S., Xu, S., Agrawral, A., Choudhury, S., Lu, Y., Tu, Z., et al. (2016). A stable room-temperature sodium–sulfur battery. *Nat. Commun.* 7 (1), 11722. doi:10.1038/ncomms11722

Weiner, S. A. (1977). "The sodium-sulfur battery: problems and promises," in *Solid state chemistry of energy conversion and storage* (Washington, D.C: American Chemical Society), 205–224.

Weller, J. M., Li, M. M., Polikarpov, E., Han, K. S., Kidner, N., Patel, A., et al. (2023). Unlocking the NaCl-$AlCl_3$ phase diagram for low-cost, long-duration Na-Al batteries. *Energy Storage Mater.* 56, 108–120. doi:10.1016/j.ensm.2023.01.009

Wentker, M., Greenwood, M., Asaba, M. C., and Leker, J. (2019a). A raw material criticality and environmental impact assessment of state-of-the-art and post-lithium-ion cathode technologies. *J. Energy Storage* 26, 101022. doi:10.1016/j.est.2019.101022

Wentker, M., Greenwood, M., Asaba, M. C., and Leker, J. (2019b). A raw material criticality and environmental impact assessment of state-of-the-art and post-lithium-ion cathode technologies. *J. Energy Storage* 26, 101022. doi:10.1016/j.est.2019.101022

Wenzel, S., Leichtweiss, T., Weber, D. A., Sann, J., Zeier, W. G., and Janek, J. (2016). Interfacial reactivity benchmarking of the sodium ion conductors Na_3PS_4 and sodium β-alumina for protected sodium metal anodes and sodium all-solid-state batteries. *ACS Appl. Mat. Interfaces* 8 (41), 28216–28224. doi:10.1021/acsami.6b10119

Whittingham, M. S., and Huggins, R. A. (1971a). Measurement of sodium ion transport in beta alumina using reversible solid electrodes. *J. Chem. Phys.* 54 (1), 414–416. doi:10.1063/1.1674623

Whittingham, M. S., and Huggins, R. A. (1971b). Transport properties of silver beta alumina. *J. Electrochem. Soc.* 118 (1), 1. doi:10.1149/1.2407944

Xu, J., Kjos, O. S., Osen, K. S., Martinez, A. M., Kongstein, O. E., and Haarberg, G. M. (2016). Na-Zn liquid metal battery. *J. Power Sources* 332, 274–280. doi:10.1016/j.jpowsour.2016.09.125

Xue, L., Xin, S., Goodenough, J. B., and Angell, C. A. (2017). An inverse aluminum battery: putting the aluminum as the cathode. *ACS Energy Lett.* 2 (7), 1534–1538. doi:10.1021/acsenergylett.7b00234

Yang, F., Mousavie, S. M. A., Oh, T. K., Yang, T., Lu, Y., Farley, C., et al. (2018). Sodium–sulfur flow battery for low-cost electrical storage. *Adv. Energy Mater.* 8 (11), 1701991. doi:10.1002/aenm.201701991

Youngblood, G. E., Miller, G. R., and Gordon, R. S. (1978). Relative effects of phase conversion and grain size on sodium ion conduction in polycrystalline, lithia-stabilized β-alumina. *J. Am. Ceram. Soc.* 61 (1-2), 86–87. doi:10.1111/j.1151-2916.1978.tb09238.x

Yuan, M., Thellufsen, J. Z., Lund, H., and Liang, Y. (2021). The electrification of transportation in energy transition. *Energy* 236, 121564. doi:10.1016/j.energy.2021.121564

Yung-Fang Yu, Y., and Kummer, J. T. (1967). Ion exchange properties of and rates of ionic diffusion in beta-alumina. *J. Inorg. Nucl. Chem.* 29 (9), 2453–2475. doi:10.1016/0022-1902(67)80301-4

Zhan, X., Bonnett, J. F., Engelhard, M. H., Reed, D. M., Sprenkle, V. L., and Li, G. (2020b). A high-performance Na–Al battery based on reversible $NaAlCl_4$ catholyte. *Adv. Energy Mater.* 10 (40), 2001378. doi:10.1002/aenm.202001378

Zhan, X., Bowden, M. E., Lu, X., Bonnett, J. F., Lemmon, T., Reed, D. M., et al. (2020a). A low-cost durable Na-$FeCl_2$ battery with ultrahigh rate capability. *Adv. Energy Mater.* 10 (10), 1903472. doi:10.1002/aenm.201903472

Zhang, Q., Lu, Y., Guo, W., Shao, Y., Liu, L., Lu, J., et al. (2021). Hunting sodium dendrites in NASICON-based solid-state electrolytes. *Energy Mat. Adv.* 2021, 1–10. doi:10.34133/2021/9870879

Zhang, Q., Lu, Y., Yu, H., Yang, G., Liu, Q., Wang, Z., et al. (2020b). PEO-$NaPF_6$ blended polymer electrolyte for solid state sodium battery. *J. Electrochem. Soc.* 167 (7), 070523. doi:10.1149/1945-7111/ab741b

Zhang, S., Quan, B., Zhao, Z., Zhao, B., He, Y., and Chen, W. (2004). Preparation and characterization of NASICON with a new sol–gel process. *Mater. Lett.* 58 (1), 226–229. doi:10.1016/S0167-577X(03)00450-6

Zhang, Z., Wenzel, S., Zhu, Y., Sann, J., Shen, L., Yang, J., et al. (2020a). $Na_3Zr_2Si_2PO_{12}$: a stable Na+-ion solid electrolyte for solid-state batteries. *ACS Appl. Energy Mater.* 3 (8), 7427–7437. doi:10.1021/acsaem.0c00820

Zhou, H., Li, H., Gong, Q., Yan, S., Zhou, X., Liang, S., et al. (2022). A sodium liquid metal battery based on the multi-cationic electrolyte for grid energy storage. *Energy Storage Mater.* 50, 572–579. doi:10.1016/j.ensm.2022.05.032

Zhou, W., Li, Y., Xin, S., and Goodenough, J. B. (2017). Rechargeable sodium all-solid-state battery. *ACS Cent. Sci.* 3, 52–57. doi:10.1021/acscentsci.6b00321

Zhu, Y. G., Leverick, G., Accogli, A., Gordiz, K., Zhang, Y., and Shao-Horn, Y. (2022b). A high-rate and high-efficiency molten-salt sodium–oxygen battery. *Energy & Environ. Sci.* 15 (11), 4636–4646. doi:10.1039/D2EE01774A

Zhu, Z., Jiang, T., Ali, M., Meng, Y., Jin, Y., Cui, Y., et al. (2022a). Rechargeable batteries for grid scale energy storage. *Chem. Rev.* 122 (22), 16610–16751. doi:10.1021/acs.chemrev.2c00289